

NUMERICAL METHOD FOR CONFORM REFLECTION

A THESIS SUBMITTED TO
THE GRADUATE SCHOOL OF APPLIED MATHEMATICS
OF
MIDDLE EAST TECHNICAL UNIVERSITY

BY

ANDRIY KUSHNAROV

IN PARTIAL FULFILLMENT OF THE REQUIREMENTS
FOR
THE DEGREE OF MASTER OF SCIENCE
IN
SCIENTIFIC COMPUTING

JANUARY 2010

Approval of the thesis:

NUMERICAL METHOD FOR CONFORM REFLECTION

submitted by **ANDRIY KUSHNAROV** in partial fulfillment of the requirements for the degree of **Master of Science in Department of Scientific Computing, Middle East Technical University** by,

Prof. Dr. Ersan Akyıldız
Director, Graduate School of **Applied Mathematics**

Prof. Dr. Bülent Karasözen
Head of Department, **Scientific Computing**

Assist. Prof. Dr. Hakan Öktem
Supervisor, **Department of Mathematics, METU**

Examining Committee Members:

Prof. Dr. Marat Akhmet
Department of Mathematics, METU

Assist. Prof. Dr. Hakan Öktem
Institute of Applied Mathematics, METU

Assoc. Prof. Dr. Azize Hayfavi
Institute of Applied Mathematics, METU

Prof. Dr. Gerhard Wilhelm Weber
Institute of Applied Mathematics, METU

Assist. Prof. Dr. Hande Toffoli
Department of Physics, METU

Date:

I hereby declare that all information in this document has been obtained and presented in accordance with academic rules and ethical conduct. I also declare that, as required by these rules and conduct, I have fully cited and referenced all material and results that are not original to this work.

Name, Last Name: ANDRIY KUSHNAROV

Signature :

ABSTRACT

NUMERICAL METHOD FOR CONFORM REFLECTION

Kushnarov, Andriy

M.S., Department of Scientific Computing

Supervisor : Assist. Prof. Dr. Hakan Öktem

January 2010, 45 pages

Conformal map has application in a lot of areas of science, e.g., fluid flow, heat conduction, solidification, electromagnetic, etc. Especially conformal map applied to elasticity theory can provide most simple and useful solution. But finding of conformal map for custom domain is not trivial problem. We used a numerical method for building a conformal map to solve torsion problem. In addition it was considered an infinite system method to solve the same problem. Results are compared.

Keywords: Conformal Map, Numerical Methods, Torsion Problem, Infinite Systems

ÖZ

KONFORM REFLECTION İÇİN NÜMERİK METOD

Kushnarov, Andriy

Yüksek Lisans, Bilimsel Hesaplama Bölümü

Tez Yöneticisi : Prof. Dr. Hakan Öktem

Ocak 2010, 45 sayfa

Konformal mapin (Acıkorur Gönderim) akışkanlar dinamiği, ısı iletimi, donma elektromanyetik gibi bilimin birçok alanında uygulamaları bulunmaktadır. Özellikle esneklik kuramındaki en basit ve kullanışlı sonuçlar konformal map yöntemiyle bulunmaktadır. Ancak rastgele bir tanım kümesi için konformal mapin bulunması doğrudan çözülebilir bir problem değildir. Bu tezde burulma problemini çözmek için konformal mapin bulan bir nümerik metod geliştirilmiştir. Geliştirilen yöntem aynı problemin çözünü için düşünülmüş olan sonsuz sistem metoduyla karşılaştırılmıştır.

Anahtar Kelimeler: Konformal Map, Nümerik Metodlar, Burulma Problemi, Sonsuz Sistemler

To my family and my Ptashka.

ACKNOWLEDGMENTS

First I would like to thank my supervisor Assist. Prof. Dr. Hakan Öktem, who supported me during all term of my studying in METU, for his mentoring and guiding in the world of scientific computing.

I am also grateful to my co-advisor Prof. Dr. Valery N. Chekhov for his support, kindness and encouragement since last seven years.

I am indebted to Natalya for her management, support, kindness and much else.

I would like to express my deepest gratitude to my family: to my admirable father, to my lovely mother and to my dear brother.

Also, the environment of IAM (Institute of Applied Mathematics) and METU has an important place in this study and my live since last two years.

PREFACE

This thesis started life as a simple scientific research seven years ago when I studied in Taurida National 'V.I. Vernadsky' University, Simferopol, Ukraine. In that years Dr. Valery N. Chekhov was my scientific advisor. Thanks to his support and deep knowledge in theory of elasticity and numerical methods this simple research became a thesis for master degree in Taurida National 'V.I. Vernadsky' University. After finishing university I continued researches in this topic. I wrote an article in one of scientific magazines. My researches continued as a master thesis in Meadle East Technical University, Ankara, Turkey.

TABLE OF CONTENTS

ABSTRACT	iv
ÖZ	v
DEDICATION	vi
ACKNOWLEDGMENTS	vii
PREFACE	viii
TABLE OF CONTENTS	ix
LIST OF TABLES	xi
LIST OF FIGURES	xii
CHAPTERS	
1 INTRODUCTION	1
1.1 CONFORMAL MAP AND ITS APPLICATIONS	1
1.2 NUMERICAL METHODS	2
2 CONFORMAL MAP METHOD	5
2.1 PROBLEM DEFINITION	5
2.2 CONSTRUCTION OF CONFORMAL MAP	6
3 METHOD OF INFINITE SYSTEMS	10
3.1 INTRODUCTION	10
3.2 PROBLEM DEFINITION	11
3.3 REPRESENTATION OF THE SOLUTION OF DIRICHLET'S PROBLEM	11
3.4 INFINITE SYSTEM OF LINEAR ALGEBRAIC EQUATIONS	14
3.5 ASYMPTOTIC BEHAVIOR OF THE SOLUTION OF AN INFINITE SYSTEM	16
3.6 ESTIMATES OF THE SOLUTION OF THE INFINITE SYSTEM	20

3.7	ESTIMATES OF THE SOLUTION STRESS STATE OF THE PRISM	24
4	NUMERICAL METHOD	29
4.1	ALGORITHM OF SUCCESSIVE APPROXIMATION	29
4.2	IMPROVEMENTS	32
4.3	SYMMETRICAL PROFILE CASE	34
4.4	SELECTION OF INITIAL APPROXIMATION	35
4.5	SOLUTION OF TORSION PROBLEM	36
5	COMPARISON AND CONCLUSIONS	41
	REFERENCES	43

LIST OF TABLES

TABLES

Table 3.1	Comparison of asymptotic (3.26) and exact (3.25) values	18
Table 3.2	Monotonic decrease of limitants in the upper bounds and increase in the lower bounds	22
Table 3.3	The upper- and lower-bound estimates x_k and \bar{x}_k	23
Table 3.4	The estimates C^+ and C^-	24
Table 3.5	The estimates σ_{zy}^+ and σ_{zy}^- have been found by solving auxiliary systems . .	26
Table 5.1	Comparison of exact and numerical solutions	41

LIST OF FIGURES

FIGURES

Figure 2.1	Conformal map from unit disk $ \zeta < 1$ into domain S	5
Figure 3.1	Subdomains D_0 , D_1 , and D_2	11
Figure 3.2	The dependence of the sums S_k on the index k	19
Figure 3.3	Determination of the exact bounds for limitants	22
Figure 3.4	Surface $z = U(x, y)$	24
Figure 3.5	Surface $z = \sigma_{zx}(x, y)$	25
Figure 3.6	Stress σ_{zx} in the subdomain D_2	27
Figure 3.7	Local perturbation of the stress state near the point A	28
Figure 4.1	Take down points $z_{ja1}^{(0)}$ normally onto the curve L	30
Figure 4.2	Cruciform profile	38
Figure 4.3	Algorithm of successive approximations	39
Figure 4.4	Dependence of stress in inner corner on radius of curvature	40
Figure 5.1	Relative error estimation	42

CHAPTER 1

INTRODUCTION

1.1 CONFORMAL MAP AND ITS APPLICATIONS

A conformal (or angle-preserving) map between two domains is a function which preserves oriented angles between curves as well as their direction. Such function preserves both angles and the shapes of infinitesimally small figures, but not necessarily their size. Conformal mapping has for more than a century, been powerful tool in mathematics, engineering, physics and a lot of other subjects of the science, especially in solving various partial differential equations (PDEs).

Some classical applications of conformal mappings to steady state problems of mathematical physics and especially for the solution of the Laplace equation can be traced to the beginning of the twentieth century. A noteworthy contribution to the theory of elasticity is by Muskhelishvili [32]. Modern contributions can be found in areas of fluid flow, heat conduction, solidification, electromagnetic, ion optics, acoustics, vibrations, wave guides and grid generation. To name a few; a detailed review and biography of the applications through 1972 was supplied by Laura [25]. The problem of flow and heat transfer in conduits of arbitrary shape in space vehicles was investigated by Sparrow and Haji-Sheikh [39]. This study was extended to noncircular conduits with uniform wall temperature by Casarella et al. [6]. Unsteady heat conduction problems in bars of arbitrary cross sections were investigated by Laura and Chi [26]. Ives [19] analyzed the incompressible flow between two concentric circles and computed the streamlines by using Garrick's method of conjugate functions. The problem of solidification of steady state and transient frozen layers in rectangular channels has been solved by Siegel, Goldstein and Savino [35]. In transient solidification the shape

of a frozen region is determined by mapping it onto a potential plane and then computing the time-dependent conformal map between the potential and the physical plane. The thermoelastic problem of uniform heat flow distributed by an isolated hole of ovaloid form was investigated by Florence and Goodier [12] and extended by Deresiewicz [9] to holes which are mapped onto the unit circle and approximated by polynomials.

Conformal mapping has been applied to acoustic waveguides of complicated cross section where the Galerkin method is applied to obtain a functional approximation for the solution of the boundary value problem. The grain of a solid propellant rocket motor with a starlike internal propagation is in the form of a circular cylinder bounded by a thin case. To solve any boundary value or eigenvalue problem, the grain cross section is conformally mapped onto a circle or an annulus. Studies on the shear vibrations of such rocket motors were done by Baltrukonis et al. [4] and Laura and Shahady [27]. Conformal mapping techniques are used in a study on the Rayleigh-Taylor instability for ideal fluid by Menikoff and Zemach [30, 31]. Grid generation for cascades of blades and inlet flows has been investigated by Inoue [17, 18]. Other contemporary applications can be found in the book on numerical conformal mapping edited by Trefethen [40].

1.2 NUMERICAL METHODS

The oldest known transformation was used by Claudius Ptolemy (ca. 150 A.D.). This mapping is known as the stereographic projection of the sphere and it represents the celestial sphere. In a totally different mapping of a sphere onto a plane, known as Mercator's projection, the spherical earth is cut along a meridian circle and conformally mapped to a plane strip and published in 1569. Even till now all sea maps are constructed by this method. In 1851 Riemann made a breakthrough in conformal mapping theory. He gave a fundamental result, known as the Riemann mapping theorem, which has since been a turning point for all subsequent developments in the theory of conformal mapping.

Since then a lot of methods for building of conformal map were developed. The results of some of these methods provide us with an explicit form of a function which approximately evaluates the mapping function for a certain source region.

One major approach in developing methods for numerical conformal mapping is based on the

following interpretation of the Riemann mapping theorem: there exists a conformal mapping $f: D \rightarrow U$ with $f(z_0) = 0$ and $f'(z_0)$ nonzero real, where $z_0 \in D$, and this function has a power series expansion $f(z) = c_1(z - z_0) + \sum_{n=2}^{\infty} c_n(z - z_0)^n$, with c_1 nonzero real and $z_0 \in D$, which converges uniformly in every closed disk with center z_0 and contained in D . However, a polynomial which is a good approximation of f in D is not the same as a truncated power series. If a polynomial $p(z) = c'_1(z - z_0) + \sum_{n=2}^N (z - z_0)^n$ approximates f with accuracy $\epsilon > 0$ then it is necessary that every term of $p(z)$ must approximate the corresponding term of the power series with accuracy $\epsilon > 0$ on the set $D \cap B(z_0, R)$, where $R = |z - z_0|$ is the radius of convergence of the power series. All this means is that a polynomial p which is a good approximation of the power series starts in the same way as the power series, but the relative error in the coefficients increases with increasing n [24].

The widely used current computational techniques are based on the integral equation methods where an integral equation is developed to relate the boundaries of the problem region and the standard region like the unit disk. Once the boundaries are discretized at n points, the integral equation is reduced to a system of algebraic equations. The majority of researches in computational conformal mapping is basically divided in two groups: the first one, where the maps are constructed from a standard region (such as the unit disk) into the problem region, and the second, where the maps are constructed the other way around.

General methods of approximate conformal map building can be found in survey articles by A.F. Bermant and A.I. Markushevich [5], M.K. Govurin and L.V. Kantarovich [13]. Also one can check monographs by L.V. Kantarovich and V.I. Krilov [21], V. Kopenfels and F. Shtalman [23], P.F. Filchakov [11] et al.

There are several types of approximate methods for building the mapping function $z = \omega(\zeta)$ – analytical, graphical-analytical and experimental-analytical. In these methods approximate expression of mapping function is built as polynomial

$$z = \omega(\zeta) = \sum_{k=1}^m C_k \zeta^k \quad (1.1)$$

where, in general, coefficients $C_k = \alpha + i\beta$ are complex. In general, representation of approximate mapping as a polynomial (1.1) makes solution of boundary-value problems appreciably easy. The most easy solution of boundary-value problem can be found exactly when the conformal mapping is represented as a polynomial of ζ powers.

There was developed an alternative method for building of interpolation polynomials for simply connected and biconnected regions using Lagrange polynomials. Also it was designed the methodology for constructing of successive approximations with adding intermediate nodes. Description of this method can be found in work by A.G. Ugodchikov [41].

In this thesis we introduced an algorithm for building conformal map numerically. In Chapter 2 the way of approximation of conformal map by polynomial is presented. There is a description of infinite systems method in Chapter 3. In Chapter 4 we introduced an algorithm of successive approximations for conformal map building. Finally we compare solutions received by numerical algorithm and infinite systems method.

CHAPTER 2

CONFORMAL MAP METHOD

2.1 PROBLEM DEFINITION

Let us consider the most simple problem – a problem of approximating to a function $z = \omega(\zeta)$. This function is conformal map from unit disk $|\zeta| < 1$ into the domain S of complex plane $z = x + iy$. The domain S is bounded by piecewise-smooth contour \bar{L} . Let the origin of coordinates for the plane z be inside \bar{L} . We will normalize conformal map in the way such that the center of the unit disk $\zeta = \zeta_0 = 0$ maps to $z = z_0 = 0 \in S$ and the point A_m of the boundary γ of the unit disk with the complex coordinates $\zeta_m = 1$ maps to M_m from the boundary of S (Fig. 2.1).

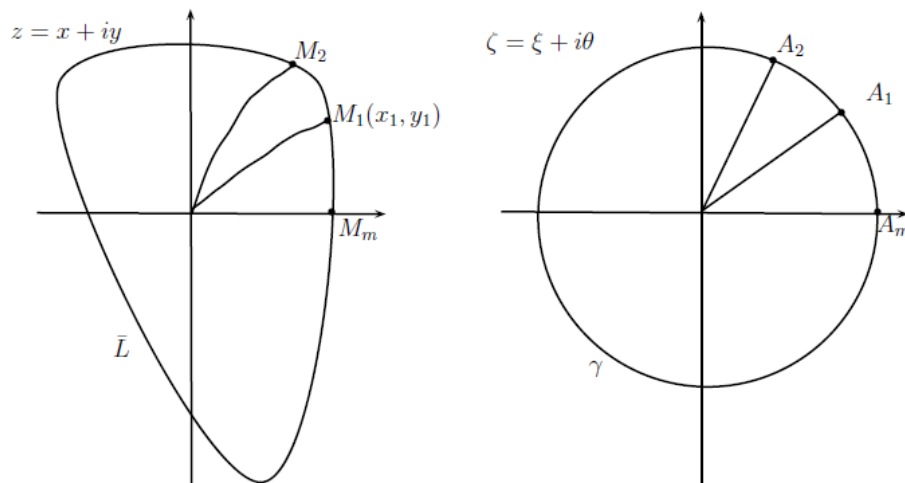


Figure 2.1: Conformal map from unit disk $|\zeta| < 1$ into domain S

Building the conformal map we will keep in mind the theorem [42].

Theorem 2.1.1 *Let Σ be finite or infinite simply connected domain on the complex plane $z = x + iy$ with the simple closed boundary. Let $\omega(\sigma)$ be function regular in Σ and continuous up to a boundary. Let point z defined by $z = \omega(\zeta)$ circumscribe simple closed circuit \bar{L} when ζ circumscribe circuit γ . Then relation $z = \omega(\zeta)$ is conformal map from S (enclosed within \bar{L}) into Σ .*

A polynomial of positive degrees is a regular function in unit disk $|\zeta| \leq 1$. So we will search for approximation of conformal map that maps unit disk $|\zeta| < 1$ into domain S as a polynomial

$$z = \omega_m(\zeta) = \sum_{k=1}^m C_k \zeta^k. \quad (2.1)$$

This means that we have to find coefficients $C_k = \alpha_k + i\beta_k (k = 1, \dots, m)$ such that curve L' (with the parametric equation $z = \omega_m(e^{i\theta})$):

- will not have double points and cusps,
- will have set of common points with the boundary \bar{L} ,
- deflection of curve L' from boundary \bar{L} of domain S should be in tolerable limit.

Note that conformity is violated in the corner points. So the exact mapping of corner points (at least two-tangent points) by the polynomial (2.1) is impossible. Because of this the piecewise smooth boundary \bar{L} should be transformed into curve L with the continuously changing tangent. In general corners of \bar{L} can be rounded by arcs of constant radius. Such rounding can be found in real world, for example in machine elements and structural engineering.

2.2 CONSTRUCTION OF CONFORMAL MAP

Let $A_j (j = 1, \dots, m)$ be points equispaced on the border γ – the boundary of unit disk. Let these points have complex coordinates $\zeta_j = e^{i\theta_j}$, where $\theta_j = \frac{2\pi}{m}j (j = 1, \dots, m)$. Suppose for a while that we know location of points M_j with coordinates $z_j = x_j + iy_j$ such that A_j are transformed into M_j by the conformal map of unit disk $|\zeta| < 1$ to domain S (Fig. 2.1).

To solve the problem of approximate conformal map we should construct the polynomial (2.1) such that

- at $\zeta = 0$ it will be zero ($z = 0$ – first normalization condition),
- at ζ_j ($j = 1, \dots, m$) it will be equal to given z_j ($j = 1, \dots, m$).

Note that value of z_m is the second normalization condition, other z_j ($j = 1, \dots, m$) are unique but previously not known.

It is easy to see that this problem is the same as the problem of construction of interpolation Lagrange polynomial $f_n(\zeta)$. In interpolation nodes ζ_j ($j = 1, \dots, m$) the Lagrange polynomial possesses the values $f(\zeta_j) = f_j$. This polynomial can be written as

$$f_n(\zeta) = \sum_{j=1}^m f_j \frac{A(\zeta)}{A'(\zeta_j)(\zeta - \zeta_j)}, \quad (2.2)$$

where

$$A(\zeta) = \prod_{j=1}^m (\zeta - \zeta_j). \quad (2.3)$$

We should keep in mind the normalization condition $\omega(0) = 0$. Now we will construct the Lagrange polynomial:

$$\omega_m(\zeta) = \sum_{k=0}^m C_k \zeta^k. \quad (2.4)$$

This polynomial will match to values of conformal map $z = \omega(\zeta)$ in interpolation nodes $\zeta = \zeta_0 = 0$ and $\zeta = \zeta_j = \exp(i\theta_j)$ ($j = 1, \dots, m$). It is easy to see that polynomial (2.4) will be

$$z = \omega_m(\zeta) = \sum_{j=0}^m z_j \frac{A(\zeta)}{A'(\zeta_j)(\zeta - \zeta_j)}, \quad (2.5)$$

where

$$A(\zeta) = \prod_{j=0}^m (\zeta - \zeta_j) = \zeta \prod_{j=1}^m (\zeta - \zeta_j). \quad (2.6)$$

We know that $\zeta_j = \sqrt[m]{-1} = \exp\left(i\frac{2\pi}{m}j\right)$ ($j = 1, \dots, m$), so

$$A(\zeta) = \zeta(\zeta^m - 1), \quad (2.7)$$

$$A'(\zeta_j) = m. \quad (2.8)$$

After substitution (2.7) and (2.8) into (2.5) we have

$$z = \omega_m(\zeta) = \frac{1 - \zeta^m}{m} \sum_{j=1}^m \frac{\zeta}{\zeta_j} \frac{z_j}{1 - \bar{\zeta}_j \zeta}. \quad (2.9)$$

Inside the unit disk $|\zeta| < 1$ it is true

$$\frac{z_j}{1 - \bar{\zeta}_j \zeta} = 1 + \bar{\zeta}_j \zeta + (\bar{\zeta}_j \zeta)^2 + \dots + (\bar{\zeta}_j \zeta)^{m-1} + \dots \quad (2.10)$$

Note that $\bar{\zeta}_j^k = \bar{\zeta}_j^{k+m}$. After substitution (2.10) into (2.9) we have

$$z = \omega_m(\zeta) = \frac{1}{m} \sum_{j=1}^m z_j [\bar{\zeta}_j \zeta + (\bar{\zeta}_j \zeta)^2 + \dots + (\bar{\zeta}_j \zeta)^m]. \quad (2.11)$$

After simple cancellation in (2.11) we will get

$$\omega_m(\zeta) = \sum_{k=1}^m C_k \zeta^k, \quad (2.12)$$

where

$$C_k = \alpha_k + i\beta_k = \frac{1}{m} \sum_{j=1}^m z_j e^{-ik\theta_j} \quad (k = 1, \dots, m). \quad (2.13)$$

Polynomial (2.12) satisfies normalization conditions and the boundary L' with the equation $z = \omega_m(\zeta)$ has at least m nodes in common with L a boundary of simply connected domain S .

After simple cancellation of real and imaginary parts in (2.13) we have

$$\begin{cases} \alpha_k = \frac{1}{m} \sum_{j=1}^m (x_j \cos \frac{2\pi}{m}kj + y_j \sin \frac{2\pi}{m}kj), \\ \beta_k = \frac{1}{m} \sum_{j=1}^m (y_j \cos \frac{2\pi}{m}kj - x_j \sin \frac{2\pi}{m}kj). \end{cases} \quad (2.14)$$

After calculation of coefficients C_k ($k = 1, \dots, m$) we should build boundary L' . We should also be sure that curve does not have double points and cusps, and deflection of curve L' from boundary L is in tolerable limit.

We can conclude that in case of known nodes M_j ($j = 1, \dots, m$) from boundary L process of construction of approximate conformal map as an interpolation polynomial is easy.

The problem of match making between nodes of boundaries γ and L is separate and difficult problem by itself. In particular it is nearly impossible to predefine this match exactly. Because of this we will use the approximate methods of determining this match. Another way is algorithm which conjectures the first approximation and then let us obtain more accurate location of such points.

Similarly to polynomial (2.12) we will build another approximation polynomial

$$\omega_{m^*}(\zeta) = \sum_{k=1}^m C_{k^*} \zeta^k \quad (2.15)$$

such that it matches to values of conformal map $z = \omega(\zeta)$ in interpolation nodes $\zeta = \zeta_0 = 0$ and $\zeta = \zeta_{j^*} = \sqrt[m]{-1} = e^{i\theta_j}$, where $\theta_j^* = \frac{\pi}{m}(2j-1)$ ($j = 1, \dots, m$). On the picture (2.1) interpolation nodes $\zeta = \zeta_{j^*}$ are marked as A_{j^*} . These nodes are called intermediate and corresponding nodes M_{j^*} on boundary L have coordinates z_{j^*} .

In the same way as for polynomial (2.5) we can find

$$z = \omega_{m^*}(\zeta) = \sum_{j=0}^m z_{j^*} \frac{A(\zeta)}{A'(\zeta_{j^*})(\zeta - \zeta_{j^*})}, \quad (2.16)$$

where

$$A(\zeta) = \zeta(\zeta^m + 1), \quad (2.17)$$

$$A'(\zeta_{j^*}) = -m. \quad (2.18)$$

After elementary cancellation in (2.16) we have formulas for coefficients of polynomial (2.15)

$$C_{k^*} = \alpha_{k^*} + i\beta_{k^*} = \frac{1}{m} \sum_{k=1}^m z_{j^*} e^{-ik\theta_{j^*}} \quad (k = 1, \dots, m). \quad (2.19)$$

This formula is the same as

$$\begin{cases} \alpha_{k^*} = \frac{1}{m} \sum_{j=1}^m (x_{j^*} \cos \frac{\pi}{m}(2j-1)k + y_{j^*} \sin \frac{\pi}{m}(2j-1)k), \\ \beta_{k^*} = \frac{1}{m} \sum_{j=1}^m (y_{j^*} \cos \frac{\pi}{m}(2j-1)k - x_{j^*} \sin \frac{\pi}{m}(2j-1)k). \end{cases} \quad (2.20)$$

CHAPTER 3

METHOD OF INFINITE SYSTEMS

3.1 INTRODUCTION

The problem of torsion of a polygonal-base prism was reduced in [2] to the numerical solution of completely regular infinite systems of linear algebraic equations. Studies on this subject are reviewed in the monograph [3]. The theory of regular and quasiregular infinite systems applied to other problems in the mechanics of elastic bodies is addressed in references [14, 15, 16, 21, 22, 29, 20, 28, 36, 37, 38]. The torsion of a cross-base prism is studied in [1, 3]. Not very accurate solutions of infinite systems allow a satisfactory assessment of the torsional stiffness of a prism, but do not allow a reliable analysis of the stress state, especially in the neighborhood of the vertex of the reentrant angle.

The limitants method was proposed in [22] to estimate solutions of regular infinite systems of linear algebraic equations. The applications of the method are reviewed in references [14, 21, 29, 28]. The use of the limitants method is difficult because of the necessity of solving a great number of finite systems of linear algebraic equations. More attractive is the improved reduction method [14, 15], which leads to one finite system of equations. However, this method does not allow assessing the reliability of approximate solutions. A modification of Koyalovich's limitants method that estimates the upper and lower bounds by solving only two auxiliary systems of linear algebraic equations is proposed in [7]. We will use this method here to solve the problem of torsion of a cross-base prism.

We would like to talk about method described in article [8] more detailed.

3.2 PROBLEM DEFINITION

As it was described in previous chapter Hooke's law for a prism under torsion can be written in form (4.16). The tangential stresses in the prism are expressed in terms of the Prandtl stress function (4.17). Which is determined by solving Dirichlet's problem for Poisson's equation (4.18) in the domain occupied by the prism base.

Following paper [3], we will restrict ourselves to a cross-shaped domain symmetric about the coordinate axes (Fig. 3.1). The symmetry allows us to consider three subdomains D_0 , D_1 , and D_2 with boundaries dashed (see the Fig. 3.1).

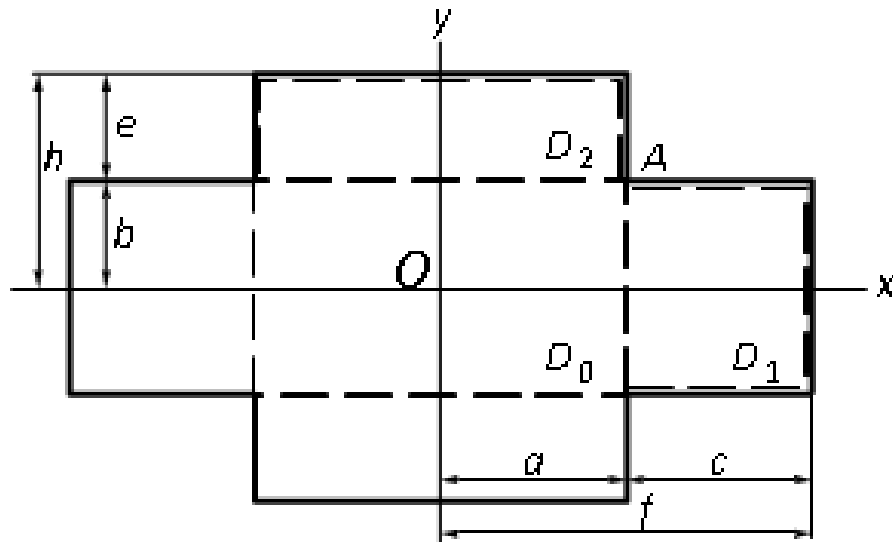


Figure 3.1: Subdomains D_0 , D_1 , and D_2

3.3 REPRESENTATION OF THE SOLUTION OF DIRICHLET'S PROBLEM

In references [1, 3], a solution was obtained by introducing a system of auxiliary functions. We will outline a different method that leads to somewhat different results.

Using partial solutions of Poisson's equation

$$\begin{aligned} U &= a^2 - x^2, (x, y) \in D_0 \cup D_2, \\ U &= b^2 - y^2, (x, y) \in D_1, \end{aligned} \quad (3.1)$$

we reduce Dirichlet's problem (4.18) to Dirichlet's problems for harmonic functions $V_i(x, y)$ in the subdomains D_0, D_1, D_2 :

$$\begin{aligned} \frac{\partial^2}{\partial x^2} V_i + \frac{\partial^2}{\partial y^2} V_i &= 0; (x, y) \in D_i, \\ V_i|_{\Gamma_i} &= F_i(x, y). \end{aligned} \quad (3.2)$$

The solution of Dirichlet's problem (3.2) for a harmonic function in a rectangular domain is described in the monograph [21]. We will reduce the solution to a series of special form having the property of Kronecker deltas relative to the values on the sides of the rectangle and formulate this as a lemma.

Lemma 3.3.1 *The solution of Dirichlet's problem for a harmonic function $V(x, y)$ in a rectangular domain ($0 < x < a$, $0 < y < b$) can be expanded into a series:*

$$\begin{aligned} V &= \sum_{n=1}^{\infty} \left\{ \left[\eta_n^{(b)} \sinh\left(n\pi \frac{y}{a}\right) + \eta_n^{(0)} \sinh\left(n\pi \frac{b-y}{a}\right) \right] \frac{\sin(n\pi x/a)}{\sinh(n\pi b/a)} \right. \\ &\quad \left. + \left[\zeta_n^{(a)} \sinh\left(n\pi \frac{x}{b}\right) + \zeta_n^{(0)} \sinh\left(n\pi \frac{a-x}{b}\right) \right] \frac{\sin(n\pi y/b)}{\sinh(n\pi a/b)} \right\}, \end{aligned}$$

where the coefficients $\eta_n^{(b)}, \eta_n^{(0)}, \zeta_n^{(b)}, \zeta_n^{(0)}$ are determined by expanding the boundary value of the function $V(x, y)$ continuous on the boundary of the rectangle into Fourier sine series:

$$\begin{aligned} V|_{y=b} &= \sum_{n=1}^{\infty} \eta_n^{(b)} \sin(n\pi x/a), & V|_{y=0} &= \sum_{n=1}^{\infty} \eta_n^{(0)} \sin(n\pi x/a), \\ V|_{x=a} &= \sum_{n=1}^{\infty} \zeta_n^{(a)} \sin(n\pi y/b), & V|_{x=0} &= \sum_{n=1}^{\infty} \zeta_n^{(0)} \sin(n\pi y/b). \end{aligned}$$

According to (3.1) the stress function in the domain D_1 is represented as

$$U_1 = b^2 - y^2 + V_1(x, y),$$

which can be used to calculate the boundary values of the harmonic function $V_1(x, y)$ on the sides $y = \pm b$ and $x = f$:

$$V_1|_{y=\pm b} = 0, \quad V_1|_{x=f} = y^2 - b^2 = \frac{-32b^2}{\pi^3} \sum_{n=1,3}^{\infty} \frac{1}{n^3} \sin\left(n\pi \frac{y+b}{2b}\right). \quad (3.3)$$

On the segment $x = a$ of the internal boundary of the subdomain D_1 , we formally expand the boundary condition into a series with unknown coefficients Y_n :

$$V_1|_{x=a} = \frac{4ab}{\pi} \sum_{n=1,3}^{\infty} \frac{1}{n} Y_n \sin\left(n\pi \frac{y+b}{2b}\right). \quad (3.4)$$

According to Lemma 3.3.1, series (3.3) and (3.4) yield a representation for the stress function $U(x, y)$ in the subdomain D_1 :

$$U_1 = b^2 - y^2 + \frac{4ab}{\pi} \sum_{n=1,3}^{\infty} \left[Y_n \sinh\left(n\pi \frac{f-x}{2b}\right) - \frac{8b}{n^2\pi^2 a} \sinh\left(n\pi \frac{x-a}{2b}\right) \right] \frac{\sin(n\pi(y+b)/(2b))}{n \sinh(n\pi c/(2b))}. \quad (3.5)$$

The solution in the subdomain D_2 is represented similarly:

$$U_1 = a^2 - x^2 + \frac{4ab}{\pi} \sum_{n=1,3}^{\infty} \left[X_n \sinh\left(n\pi \frac{h-y}{2a}\right) - \frac{8a}{n^2\pi^2 b} \sinh\left(n\pi \frac{y-b}{2a}\right) \right] \frac{\sin(n\pi(x+a)/(2a))}{n \sinh(n\pi e/(2a))}. \quad (3.6)$$

The boundary conditions for the function harmonic in the subdomain D_0 follow from the continuity of the function $U(x, y)$ on the internal boundaries $x = a$ and $y = b$

$$U_0|_{x=a} = U_1|_{x=a}, \quad U_0|_{y=b} = U_2|_{y=b}.$$

As a result, Lemma 3.3.1 leads to the following representation of the solution:

$$U_0 = a^2 - x^2 + \frac{4ab}{\pi} \sum_{n=1,3}^{\infty} \left[\frac{X_n}{n \cosh(n\pi b/(2a))} \cosh\left(n\pi \frac{y}{2a}\right) \sin\left(n\pi \frac{x+a}{2a}\right) + \frac{1}{n^3\pi^2} \frac{n^2\pi^2 Y_n + 8b/a}{\cosh(n\pi a/(2b))} \cosh\left(n\pi \frac{x}{2b}\right) \sin\left(n\pi \frac{y+b}{2b}\right) \right] \quad (3.7)$$

Integrating (3.5) – (3.7) according to (4.20), we obtain a formula for the torsional stiffness coefficient C :

$$\begin{aligned} \frac{1}{16b^4G} C &= \frac{c}{3b} + \frac{a^3h}{3b^4} + \frac{8a^3}{\pi^3 b^3} \sum_{n=1,3}^{\infty} \frac{X_n}{n^3} \left[\tanh\left(n\pi \frac{b}{2a}\right) + \tanh\left(n\pi \frac{e}{4a}\right) \right] \\ &\quad + \frac{8a}{\pi^3 b} \sum_{n=1,3}^{\infty} \frac{Y_n}{n^3} \left[\tanh\left(n\pi \frac{a}{2b}\right) + \tanh\left(n\pi \frac{c}{4b}\right) \right] \\ &\quad + \frac{64}{\pi^5} \sum_{n=1,3}^{\infty} \frac{1}{n^5} \left[\tanh\left(n\pi \frac{a}{2b}\right) + \tanh\left(n\pi \frac{c}{4b}\right) - \frac{a^4}{b^4} \tanh\left(n\pi \frac{e}{4a}\right) \right], \end{aligned} \quad (3.8)$$

where G is modulus of rigidity.

3.4 INFINITE SYSTEM OF LINEAR ALGEBRAIC EQUATIONS

The equations for the coefficients $\{X_n, Y_n\}$ follow from the smoothness of the stress function on the internal boundaries $x = a$ and $y = b$:

$$\left. \frac{\partial U_0}{\partial x} \right|_{x=a} = \left. \frac{\partial U_1}{\partial x} \right|_{x=a}, \quad \left. \frac{\partial U_0}{\partial y} \right|_{y=b} = \left. \frac{\partial U_1}{\partial y} \right|_{y=b}. \quad (3.9)$$

Substituting expressions (3.6) and (3.7) into the second condition (3.9), we get

$$\begin{aligned} & \sum_{n=1,3}^{\infty} \left\{ \left[\tanh\left(k\pi \frac{b}{2a}\right) + \coth\left(k\pi \frac{e}{2a}\right) \right] X_k + \frac{8a}{k^2 \pi^2 b \sinh\left(k\pi \frac{e}{2a}\right)} \sin\left(k\pi \frac{x+a}{2a}\right) \right\} \\ & = \frac{a}{b} \sum_{n=1,3}^{\infty} \left(Y_n + \frac{8b}{n^2 \pi^2 a} \right) \cosh\left(n\pi \frac{x}{2b}\right) / \cosh\left(n\pi \frac{a}{2b}\right) \quad (-a < x < a). \end{aligned} \quad (3.10)$$

Using the well-known [34] series for hyperbolic cosine:

$$\cosh\left(n\pi \frac{x}{2b}\right) = \frac{4}{\pi} \cosh\left(n\pi \frac{a}{2b}\right) \sum_{k=1,3}^{\infty} \frac{k}{k^2 + n^2 a^2 / b^2} \sin\left(k\pi \frac{x+a}{2a}\right) \quad (-a < x < a)$$

we represent the right-hand side of (3.10) as a Fourier sine series. Changing the order of summation (indices n and k) and equating the coefficients of the sines on the left- and right-hand sides leads to a countable set of linear algebraic equations for X_n, Y_n , which are written simultaneously with a corollary of the first continuity condition (3.9) derived similarly:

$$\begin{aligned} X_k &= \frac{4kb}{\Delta_e \pi a} \sum_{n=1,3}^{\infty} \frac{Y_n}{n^2 + k^2 b^2 / a^2} + \frac{1}{\Delta_e} \left[\frac{4}{k\pi} - \frac{8a}{k^2 \pi^2 b} \left(\tanh\left(k\pi \frac{b}{2a}\right) + 1 / \sinh\left(k\pi \frac{e}{2a}\right) \right) \right] \\ Y_k &= \frac{4ka}{\Delta_c \pi b} \sum_{n=1,3}^{\infty} \frac{X_n}{n^2 + k^2 a^2 / b^2} + \frac{1}{\Delta_c} \left[\frac{4}{k\pi} - \frac{8b}{k^2 \pi^2 a} \left(\tanh\left(k\pi \frac{a}{2b}\right) + 1 / \sinh\left(k\pi \frac{c}{2b}\right) \right) \right], \end{aligned} \quad (3.11)$$

where $k = 1, 3, 5, \dots$, $\Delta_c = \tanh\left(k\pi \frac{a}{2b}\right) + \coth\left(k\pi \frac{c}{2b}\right)$, $\Delta_e = \tanh\left(k\pi \frac{b}{2a}\right) + \coth\left(k\pi \frac{e}{2a}\right)$.

Comparing the infinite system (3.11) with the similar pair infinite system derived in [3], we can transform the matrix of one system into the matrix of the other system. The free terms have an elementary form in (3.11) and are expressed in terms of infinite series in [3].

If the parameters e and c (Fig. 3.1) are equal to zero, then the cross-shaped domain degenerates into a rectangle with sides $2a$ and $2b$. Passing to the limit as $e \rightarrow 0$ in the first equation in (3.11) and as $c \rightarrow 0$ in the second equation in (3.11), we obtain a limiting solution of the pair infinite system:

$$X_n = \frac{-8a}{n^2 \pi^2 b}, \quad Y_n = \frac{-8b}{n^2 \pi^2 a}, \quad (n = 1, 3, 5, \dots),$$

which transforms expression (3.7) for the function $U_0(x, y)$ into the well-known Prandtl's stress function for a rectangular-base prism under torsion.

If the cross-shaped domain ($c > 0, e > 0$) is nondegenerate, we use the standard notation [21] for the pair infinite systems of linear algebraic equations (with odd indices):

$$x_k = \sum_{n=1,3}^{\infty} a_{k,n} y_n + b_k, \quad y_k = \sum_{n=1,3}^{\infty} \alpha_{k,n} x_n + \beta_k \quad (k = 1, 3, 5, \dots) \quad (3.12)$$

and calculate the auxiliary infinite sequences

$$\rho_k = 1 - \sum_{n=1,3}^{\infty} |a_{k,n}|, \quad r_k = 1 - \sum_{n=1,3}^{\infty} |\alpha_{k,n}| \quad (k = 1, 3, 5, \dots). \quad (3.13)$$

Using the infinite series sum $\sum_{n=1,3}^{\infty} \frac{1}{n^2 + z^2} = \frac{\pi}{4z} \tanh(\pi z/2)$ [34], we transform sequences (3.13) to

$$\rho_k = \frac{1}{1 + \tanh\left(k\pi \frac{b}{2a}\right) \tanh\left(k\pi \frac{e}{2a}\right)}$$

$$r_k = \frac{1}{1 + \tanh\left(k\pi \frac{a}{2b}\right) \tanh\left(k\pi \frac{c}{2b}\right)}$$

$(k = 1, 3, 5, \dots).$

This yields the obvious estimates $1/2 < \rho_k < 1$ and $1/2 < r_k < 1$, which suggest that the pair infinite system (3.11) is completely regular. The free terms of system (3.11) tend to zero with increasing k . Therefore, the infinite system (3.11) has a unique bounded solution [21].

In the specific case of equal-cross base ($b = a, e = c$), the infinite system (3.11) becomes

$$X_k \Delta_c = \frac{4k}{\pi} \sum_{n=1,3}^{\infty} \frac{Y_n}{n^2 + k^2} + \frac{4}{k\pi} - \frac{8}{k^2 \pi^2} \left(\tanh\left(k \frac{\pi}{2}\right) + 1 / \sinh\left(k\pi \frac{c}{2a}\right) \right),$$

$$Y_k \Delta_c = \frac{4k}{\pi} \sum_{n=1,3}^{\infty} \frac{X_n}{n^2 + k^2} + \frac{4}{k\pi} - \frac{8}{k^2 \pi^2} \left(\tanh\left(k \frac{\pi}{2}\right) + 1 / \sinh\left(k\pi \frac{c}{2a}\right) \right). \quad (3.14)$$

Subtracting the second equation from the first one in (3.14), we see that the differences $X_k - Y_k$ satisfy the homogeneous, completely regular, infinite system

$$X_k - Y_k + \frac{4k}{\pi \Delta_c} \sum_{n=1,3}^{\infty} \frac{X_n - Y_n}{n^2 + k^2} \quad (k = 1, 3, 5, \dots),$$

which has a unique limited solution $X_k - Y_k = 0$ [21]. Therefore, the pair system (3.14) is equivalent to the following completely regular system:

$$X_k \Delta_c = \frac{4k}{\pi} \sum_{n=1,3}^{\infty} \frac{X_n}{n^2 + k^2} + \frac{4}{k\pi} - \frac{8}{k^2 \pi^2} \left(\tanh\left(k \frac{\pi}{2}\right) + 1 / \sinh\left(k\pi \frac{c}{2a}\right) \right), \quad (3.15)$$

where $k = 1, 3, 5, \dots$, $\Delta_c = \tanh\left(k\frac{\pi}{2}\right) + \coth\left(k\pi\frac{c}{2b}\right)$.

Due to symmetry, it is sufficient to use the representation of solution (3.5), (3.7) in the domains D_1 and D_0 :

$$\begin{aligned}
U_1 &= a^2 - y^2 \\
&+ \frac{4a^2}{\pi} \sum_{n=1,3}^{\infty} \left[X_n \sinh\left(n\pi\frac{f-x}{2a}\right) - \frac{8}{n^2\pi^2} \sinh\left(n\pi\frac{x-a}{2a}\right) \right] \frac{\sin(n\pi(y+a)/(2a))}{n \sinh(n\pi c/(2a))}, \\
U_0 &= a^2 - x^2 + \frac{4a^2}{\pi} \sum_{n=1,3}^{\infty} \frac{1}{n} \left[X_n \cosh\left(n\pi\frac{y}{2a}\right) \sin\left(n\pi\frac{x+a}{2a}\right) \right. \\
&\quad \left. + \left(X_n + \frac{8}{n^2\pi^2} \right) \cosh\left(n\pi\frac{x}{2a}\right) \sin\left(n\pi\frac{y+a}{2a}\right) \right] / \cosh\left(n\frac{\pi}{2}\right).
\end{aligned} \tag{3.16}$$

3.5 ASYMPTOTIC BEHAVIOR OF THE SOLUTION OF AN INFINITE SYSTEM

According to Chekhov [3], the tangential stresses at the point A (Fig. 3.1) have a power singularity with exponent $m = -\frac{1}{3}$. For example, the tangential stress $\sigma_{xy}|_{x=a}$ on the segment $x = a$ tends to infinity as the corner point A is approached:

$$\sigma_{xy}|_{x=a} \sim \frac{B}{(b-y)^{1/3}} \text{ as } y \rightarrow b. \tag{3.17}$$

Substituting (3.5) into formulas (4.17), we obtain expressions for the stresses in the domain D_1 :

$$\begin{aligned}
\frac{1}{2aG\theta} \sigma_{zx} &= \sum_{n=1,3}^{\infty} \left[Y_n \sinh\left(n\pi\frac{f-x}{2b}\right) - \frac{8b}{n^2\pi^2 a} \sinh\left(n\pi\frac{x-a}{2b}\right) \right] \frac{\cosh(n\pi(y+b)/(2b))}{\sinh(n\pi c/(2b))} \\
&\quad - \frac{y}{a} \\
\frac{1}{2aG\theta} \sigma_{zy} &= \sum_{n=1,3}^{\infty} \left[Y_n \cosh\left(n\pi\frac{f-x}{2b}\right) + \frac{8b}{n^2\pi^2 a} \cosh\left(n\pi\frac{x-a}{2b}\right) \right] \frac{\sinh(n\pi(y+b)/(2b))}{\sinh(n\pi c/(2b))},
\end{aligned} \tag{3.18}$$

here G is modulus of rigidity.

On the segment $x = a$, the first expression in (3.18) becomes simpler:

$$\frac{1}{2aG\theta} \sigma_{zx} = \sum_{n=1,3}^{\infty} Y_n \cos\left(n\pi\frac{y+b}{2b}\right) - \frac{y}{a}. \tag{3.19}$$

To relate the singularity order of the stresses at the corner point to the asymptotic behavior of the solution of the infinite system at large values of n , we replace variables:

$$X_n = (a/b)^{\nu/2} x_n/n^\nu, \quad Y_n = (b/a)^{\nu/2} y_n/n^\nu \quad (\nu > 0) \quad (3.20)$$

and assume that the new variables tend to a nonzero real constant at great values of n , i.e.,

$$x_n \rightarrow c_0, \quad y_n \rightarrow c_0 \quad \text{as } n \rightarrow \infty. \quad (3.21)$$

After replacement (3.20) in (3.19), we separate out the part of series segment with the constant c_0 :

$$\begin{aligned} \frac{1}{2aG\theta} \sigma_{zx} \Big|_{x=a} &= \left(\sum_{n=1,3}^{\infty} \frac{y_n - c_0}{n^\nu} \cos\left(n\pi \frac{y+b}{2b}\right) \right. \\ &\left. + \sum_{n=1,3}^{\infty} \frac{c_0}{n^\nu} \cos\left(n\pi \frac{y+b}{2b}\right) \right) \left(\frac{b}{a} \right)^{\nu/2} - \frac{y}{a}. \end{aligned} \quad (3.22)$$

The constant c_0 is taken out of last series, which can be expressed in terms of a special function $\text{Li}_\nu(z)$ called a polylogarithm of order ν [34]:

$$\begin{aligned} \sigma(\nu, y) &= - \sum_{n=1,3}^{\infty} \frac{2}{n^\nu} \cos\left(n\pi \frac{y+b}{2b}\right) \\ &= \text{Re} \left[\text{Li}_\nu\left(-\exp\left(i\pi \frac{b+y}{2b}\right)\right) - \text{Li}_\nu\left(\exp\left(i\pi \frac{b+y}{2b}\right)\right) \right]. \end{aligned} \quad (3.23)$$

The first series in (3.22) turns into a finite sum because of (3.21):

$$\sum_{n=1,3}^{\infty} \frac{y_n - c_0}{n^\nu} \cos\left(n\pi \frac{y+b}{2b}\right) \approx \sum_{n=1,3}^q \frac{y_n - c_0}{n^\nu} \cos\left(n\pi \frac{y+b}{2b}\right)$$

The error of this approximate formula can be made arbitrary small by increasing the upper limit q . Thus, transformations (3.20)-(3.23) improve the convergence of the series in (3.19).

The right-hand side of (3.23) has an asymptotic representation in the neighborhood ($y < b$) of the point A:

$$\sigma(\nu, y) = \sigma_{asym}(\nu, y) + O(1 - y/b),$$

where

$$\sigma_{asym}(\nu, y) = (2/\pi)^{1-\nu} \frac{\Gamma(1-\nu)}{(1-y/b)^{1-\nu}} \text{Re}[(-1)^{\frac{\nu-1}{2}}] + (2-2^{1-\nu})\zeta(2/3), \quad (3.24)$$

, $\Gamma(z)$ being the Gamma function; $\zeta(z)$ is the Riemann zeta function.

Comparing expressions (3.17) and (3.24), we find $\nu = 2/3$. Formulas (3.23) and (3.24) become

$$\begin{aligned}\sigma(2/3, y) &= - \sum_{n=1,3}^{\infty} \frac{2}{n^{2/3}} \cos\left(n\pi \frac{y+b}{2b}\right) \\ &= \operatorname{Re} \left[\operatorname{Li}_{2/3}\left(-\exp\left(i\pi \frac{b+y}{2b}\right)\right) - \operatorname{Li}_{2/3}\left(\exp\left(i\pi \frac{b+y}{2b}\right)\right) \right],\end{aligned}\quad (3.25)$$

$$\sigma(2/3, y) = \frac{\sqrt{3}\Gamma(1/3)}{\sqrt[3]{4\pi(1-y/b)}} + (2 - \sqrt[3]{2})\zeta(2/3).\quad (3.26)$$

Table 3.1: Comparison of asymptotic (3.26) and exact (3.25) values

y/b	0.75	0.79	0.83	0.87	0.91	0.95	0.99
$\sigma(2/3, y)$	0.59726	0.74966	0.95701	1.2558	1.7309	2.6557	6.4623
$\sigma_{asym}(2/3, y)$	0.60675	0.75634	0.96137	1.2584	1.7321	2.6561	6.4624

In table 3.1 the comparison of the asymptotic (3.26) and exact (3.25) values on the segment $(3/4b, b)$ is presented.

Using eq. (3.20) with $\nu = 2/3$ in (3.11),

$$X_n = (a/b)^{1/3} x_n/n^{2/3}, \quad Y_n = (b/a)^{1/3} y_n/n^{2/3},\quad (3.27)$$

we arrive at a pair infinite system that has a solution tending to the nonzero constant c_0 as the number n tends to infinity:

$$\begin{aligned}x_k &= \frac{4\zeta_k^{5/3}}{\Delta_e\pi} \sum_{n=1,3}^{\infty} \frac{y_n}{(n^2 + \zeta_k^2)n^{2/3}} + \frac{\sqrt[3]{k\zeta_k}}{\Delta_e} \left[\frac{4}{k\pi} - \frac{8a}{k^2\pi^2b} \left(\tanh\left(k\pi \frac{b}{2a}\right) \right. \right. \\ &\quad \left. \left. + 1/\sinh\left(k\pi \frac{e}{2a}\right) \right) \right],\end{aligned}\quad (3.28)$$

$$\begin{aligned}y_k &= \frac{4\eta_k^{5/3}}{\Delta_c\pi} \sum_{n=1,3}^{\infty} \frac{x_n}{(n^2 + \eta_k^2)n^{2/3}} + \frac{\sqrt[3]{k\eta_k}}{\Delta_c} \left[\frac{4}{k\pi} - \frac{8b}{k^2\pi^2a} \left(\tanh\left(k\pi \frac{a}{2b}\right) \right. \right. \\ &\quad \left. \left. + 1/\sinh\left(k\pi \frac{c}{2b}\right) \right) \right],\end{aligned}$$

where $\zeta_k = kb/a$ and $\eta_k = ka/b$.

To apply the limitants method, should necessarily be the infinite system regular. The pair infinite system (3.28) is regular if

$$\frac{4\zeta_k^{5/3}}{\Delta_e\pi} \sum_{n=1,3}^{\infty} \frac{y_n}{(n^2 + \zeta_k^2)n^{2/3}} < 1, \quad \frac{4\eta_k^{5/3}}{\Delta_c\pi} \sum_{n=1,3}^{\infty} \frac{x_n}{(n^2 + \eta_k^2)n^{2/3}} < 1 \quad (k = 1, 3, 5, \dots).\quad (3.29)$$

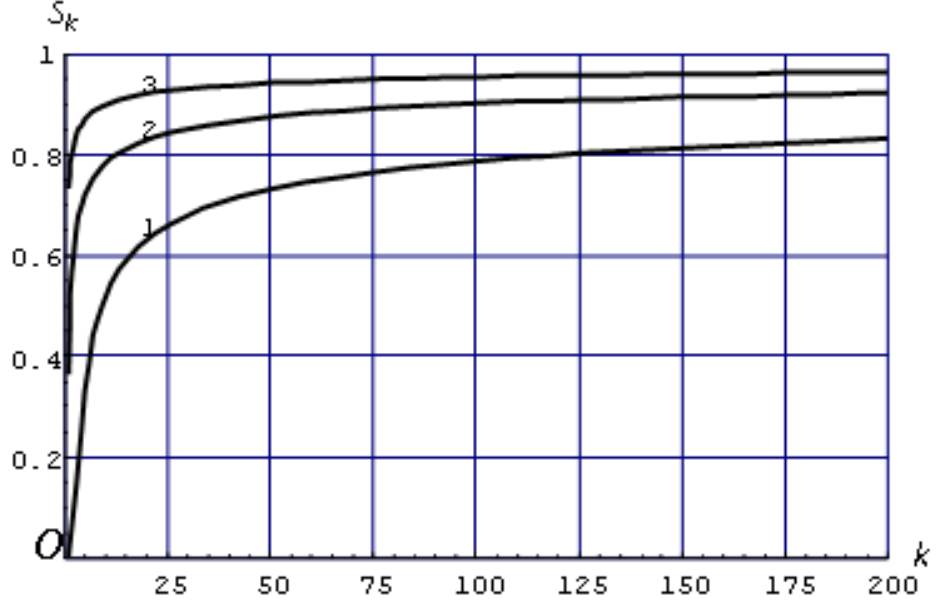


Figure 3.2: The dependence of the sums S_k on the index k

The explicit dependence of the sums of the series in (3.29) on the index k can be represented using the Euler-Maclaurin formula [10]:

$$\begin{aligned} \sum_{n=1,3}^{\infty} f(x) &= \sum_{n=1,3}^{q-2} f(x) + \frac{1}{2} \int_q^{\infty} f(x) dx + \frac{1}{2} f(q) - B_1 f^{(1)}(q) + \frac{1}{4!} B_2 2^3 f^{(3)}(q) \\ &\quad - \frac{1}{6!} B_3 2^5 f^{(5)}(q) + \dots + (-1)^{k-1} \frac{1}{(2k-2)!} B_{k-1} 2^{2k-3} f^{(2k-3)}(q) \\ &\quad + \theta (-1)^k \frac{1}{(2k)!} B_k 2^{2k-1} f^{(2k-1)}(q), \end{aligned} \quad (3.30)$$

where $0 \leq \theta \leq 1$; the odd number q is introduced to improve the asymptotic formula; $B_1 = 1/6, B_2 = 1/30, B_3 = 1/42, \dots$ are Bernoulli numbers. All the even-order derivatives $f^{(2j)}(x)$ should have the same sign within $(q, +\infty)$, and all the odd-order derivatives $f^{(2j-1)}(x)$ should tend to zero as $x \rightarrow \infty$. The error of the asymptotic formula can be estimated by comparing the results obtained with $\theta = 1$ and $\theta = 0$.

Denoting the first series in (3.29) by S_k and using four terms of the asymptotic formula (3.30), we obtain

$$\begin{aligned} S_k &= \frac{4\zeta_k^{5/3}}{\Delta_e \pi} \left\{ \sum_{n=1,3}^{q-2} \frac{1}{(n^2 + \zeta_k^2) n^{2/3}} + \frac{1}{4\zeta_k^{5/3}} \left[\arctan\left(\frac{\zeta_k}{q}\right) \right. \right. \\ &\quad \left. \left. 3 \arctan(\sqrt[3]{\zeta_k/q}) + \frac{\sqrt{3}}{2} \ln \left(\frac{1 + (2\sqrt[3]{q/\zeta_k} - \sqrt{3})^2}{1 + (2\sqrt[3]{q/\zeta_k} + \sqrt{3})^2} \right) \right] \right. \\ &\quad \left. + \frac{1}{2(q^2 + \zeta_k^2) q^{2/3}} + \frac{1}{6} \left(\frac{2q^{1/3}}{(q^2 + \zeta_k^2)^2} + \frac{2}{3(q^2 + \zeta_k^2) q^{5/3}} \right) \right\}. \end{aligned} \quad (3.31)$$

This is an upper-bound estimate of the sum. The lower-bound estimate is obtained by rejecting the last expression in brackets multiplied by $1/6$ in (3.31). The upper- and lower-bound estimates are made to coincide in the first five decimal places by choosing the value $q = 201$. The dependence of the sums S_k on the index k is shown in Fig. 3.2. Curve 1 corresponds to $b/a = 1/10$, curve 2 to $b/a = 1$, and curve 3 to $b/a = 10$ (for $e = b$). The similarity between the two series in (3.29) allows us to interpret curve 3 as dependence of the sum of the second series with $a/b = 1/10$ and $c = a$ on the index k . Thus, the curves in Fig. 3.2 show that the sums of series (3.29) asymptotically tend to the limiting value $S_k = 1$ from below. Note that the limit $\lim_{x \rightarrow \infty} S_k = 1$ can be evaluated in an elementary way using formula (3.31). Thus, the pair infinite system (3.28) appears regular.

Note that the uniqueness of a bounded solution of system (3.28) from the reversibility of transformation (3.27), which establishes one-to-one correspondence between any bounded solution of system (3.28) and the unique solution of the pair regular system (3.11) that tends to zero.

The stress state of an angle subject to torsion was studied in the article of Chekhov [33], which was the first to use a transformation of the form (3.27) for variables in the case where $b = a$.

3.6 ESTIMATES OF THE SOLUTION OF THE INFINITE SYSTEM

Estimates of the Solution of the Infinite System. We will restrict ourselves to the special case of an equal-cross base ($b = a$, $e = c$, and $h = f$). It was shown in before that the pair infinite system (3.28) can be replaced by a regular infinite system of the form (3.15):

$$x_k = \frac{4k^{5/3}}{\Delta_c \pi} \sum_{n=1,3}^{\infty} \frac{x_n}{(n^2 + k^2)n^{2/3}} + b_k, \quad (3.32)$$

where

$$b_k = \frac{k^{2/3}}{\Delta_c} \left[\frac{4}{k\pi} - \frac{8}{k^2\pi^2} (\tanh(k\pi/2) + 1/\sinh(k\pi/2)) \right], \quad (3.33)$$

$$\Delta_c = \tanh(k\pi/2) + \coth(k\pi/2), \quad k = 1, 3, 5, \dots, \quad \gamma = c/a.$$

According to [7], to estimate the lower and upper bounds for the solution of the regular infinite system (3.32), it is necessary to find the solutions of two auxiliary finite systems

($k = 1, 3, \dots, 2p - 1$):

$$\begin{aligned}\check{x}_k &= \frac{4k^{5/3}}{\Delta_c \pi} \sum_{n=1,3}^{2p-1} \frac{\check{x}_n}{(n^2 + k^2)n^{2/3}} + b_k, \\ \tilde{x}_k &= \frac{4k^{5/3}}{\Delta_c \pi} \sum_{n=1,3}^{2p-1} \frac{\tilde{x}_n}{(n^2 + k^2)n^{2/3}} + \tilde{b}_k,\end{aligned}\quad (3.34)$$

where

$$\tilde{b}_k = \frac{4k^{5/3}}{\Delta_c \pi} \sum_{n=2p+1}^{\infty} \frac{1}{(n^2 + k^2)n^{2/3}}. \quad (3.35)$$

The solutions of the auxiliary systems are substituted into the following expression for the "limiting" limitant V_k^{*p} for system (3.32):

$$V_k^{*p} = \left(b_k + \sum_{n=1,3}^{2p-1} a_{k,n} \check{x}_n \right) \left/ \left(\rho_k + \sum_{n=1,3}^{2p-1} a_{k,n} (1 - \check{x}_n) \right) \right. . \quad (3.36)$$

Substituting the free terms (3.33) and the coefficients of (3.32) and performing reduction, we get

$$V_k^{*p} = \frac{1 - \frac{2}{\pi k} \left[\tanh\left(k\frac{\pi}{2}\right) + 1/\sinh\left(k\pi\frac{\gamma}{2}\right) \right] + \sum_{n=1,3}^{2p-1} \frac{\check{x}_n}{(n^2/k^2 + 1)n^{2/3}}}{\frac{\pi}{4} k^{1/3} \left[\tanh\left(k\frac{\pi}{2}\right) + 1/\sinh\left(k\pi\frac{\gamma}{2}\right) \right] + S}, \quad (3.37)$$

where

$$S = - \sum_{n=2p+1}^{\infty} \frac{1}{(n^2/k^2 + 1)n^{2/3}} + \sum_{n=1,3}^{2p-1} \frac{\tilde{x}_n}{(n^2/k^2 + 1)n^{2/3}}.$$

The sum of the infinite series in the denominator is again calculated by the Euler-Maclaurin formula (3.30). It is desirable to find a limiting expression of limitant (3.37) as $k \rightarrow \infty$. It has the form

$$V_{inf}^{*p} = \left(1 + \sum_{n=1,3}^{2p-1} \frac{\check{x}_n}{n^{2/3}} \right) \left/ \left(q^{1/3} \text{asym}(q) - \sum_{n=2p+1}^{q-2} \frac{1}{n^{2/3}} - \sum_{n=1,3}^{2p-1} \frac{\check{x}_n}{n^{2/3}} \right) \right. ,$$

$$\text{where } \text{asym}(q) = \frac{3}{2} - \frac{1}{2q} - \frac{2b_1}{3q^2} + \frac{80b_2}{81q^4} - \frac{4928b_3}{2187q^6} + \frac{119680b_4}{19683q^8} - \frac{28627456b_5}{1594323q^{10}} + O(q^{-12}).$$

The exact lower and upper bounds for (3.37)

$$h^{*p} = \inf_{k \geq 2p+1} V_k^{*p}, \quad H^{*p} = \sup_{k \geq 2p+1} V_k^{*p}. \quad (3.38)$$

allow us [7] to estimate the lower and upper bounds for the variables:

$$\begin{aligned}\bar{x}_k &= \check{x}_n + h^{*p} \tilde{x}_n \leq x_n \leq \check{x}_n + H^{*p} \tilde{x}_n \quad (n = 1, 3, \dots, 2p - 1), \\ h^{*p} &\leq x_n \leq H^{*p} \quad (n \geq 2p + 1).\end{aligned}\quad (3.39)$$

The solutions of the auxiliary systems (3.34) can also be associated with the improved reduction method. It is assumed that the approximate equalities $x_n \approx c_0$ hold beginning with $2p + 1$. Then the first p equations in (3.32) form a linear system whose free terms are linear combinations of the free terms (3.33) and (3.36) of the auxiliary systems (3.34):

$$x_k = \frac{4k^{5/3}}{\Delta_c \pi} \sum_{n=1,3}^{2p-1} \frac{x_n}{(n^2 + k^2)n^{2/3}} + c_0 \tilde{b}_k + b_k. \quad (3.40)$$

Accordingly, the solution of the linear system (3.40) is represented by the same linear combination of solutions of these auxiliary systems:

$$\check{x}_n = \check{x}_n + c_0 \tilde{x}_n \quad (n = 1, 3, \dots, 2p - 1). \quad (3.41)$$

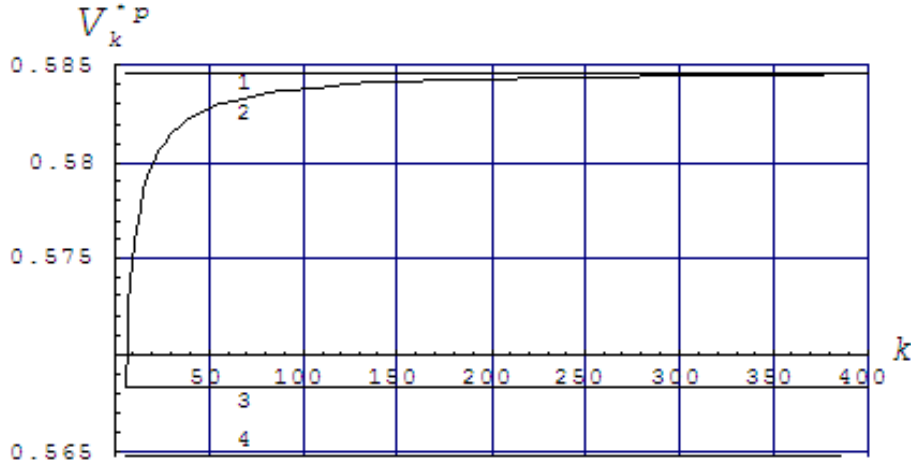


Figure 3.3: Determination of the exact bounds for limitants

The unknown c_0 can be calculated, additionally assuming that \check{x}_{2p-1} . Then the last equation in (3.41) yields

$$c_0 = \check{x}_{2p-1} / (1 - \tilde{x}_{2p-1}). \quad (3.42)$$

Table 3.2: Monotonic decrease of limitants in the upper bounds and increase in the lower bounds

p	5	30	100	500	2000
H^*p	0.584784	0.580679	0.580352	0.580284	0.580279
h^*p	0.568374	0.579047	0.580026	0.580254	0.580273
c_0	0.564796	0.578991	0.580023	0.580254	0.580273

A typical property of limitants is [22] monotonic decrease in the upper bounds (3.38) and increase in the lower bounds with increase in the order p of the auxiliary systems. Table 3.2 illustrates this property for some values of p (for $\gamma = 1$). For comparison, the table includes a row of values of c_0 calculated by formula (3.42) corresponding to the improved reduction method.

It follows from Table 3.2 that the lower-bound estimate produced by the improved reduction method is worse than that by the limitants method. As p increases, both lower-bound estimates tend to each other (in this example).

The use of a limitant curve facilitates the determination of the exact bounds for limitants.

Such a curve is shown in Fig. 3.3 for $2 = 1, p = 5$, and $q = 201$. Lines 1, 3, and 4 represent the estimates from the first column of Table 3.2, while curve 2 corresponds to limitant (3.37) for $k \geq 6$.

The upper- and lower-bound estimates x_k and \bar{x}_k (3.39) are illustrated by Table 3.3 for the case where the order of the auxiliary systems is equal to five ($\gamma = 1$).

Between the upper- and lower-bound estimates (3.39) there is a row of values of the exact solution x_k^* obtained using auxiliary systems of higher order.

For comparison, the table includes the solution \check{x}_k produced by the improved reduction method.

It follows from Tables 3.2 and 3.3 that the difference between the upper- and lower-bound estimates increases with the variable number, reaching the maximum values for the limiting estimates H^{*p} and h^{*p} .

Table 3.3: The upper- and lower-bound estimates x_k and \bar{x}_k

k	1	3	5	7	9	11
$10x_k$	1.6733	5.2041	5.5069	5.6185	5.6770	5.8478
$10x_k^*$	1.6722	5.1998	5.4987	5.6064	5.6613	5.6940
$10\bar{x}_k$	1.6717	5.1978	5.4948	5.6004	5.6532	5.6837
$10\check{x}_k$	1.6714	5.1964	5.4921	5.5964	5.6480	5.6480

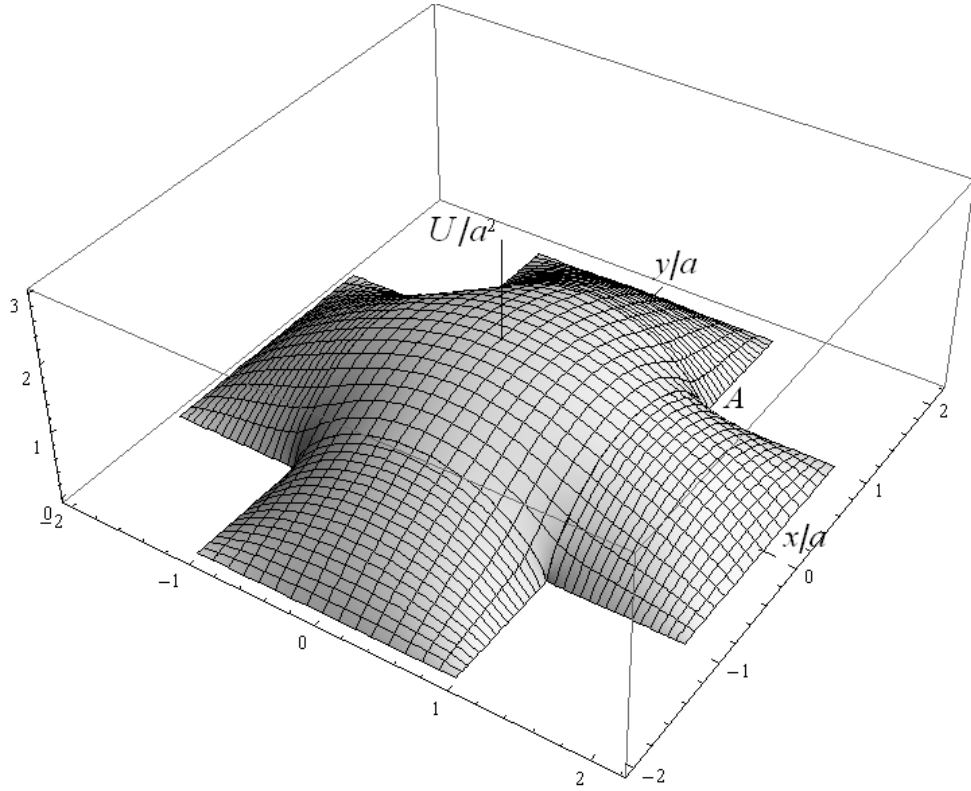


Figure 3.4: Surface $z = U(x, y)$

3.7 ESTIMATES OF THE SOLUTION STRESS STATE OF THE PRISM

It is not difficult to calculate the stress function inside the prism base after the substitution of the lower- and upper-bound estimates for the solution of the infinite system into (3.16). Only on the boundary does the exponential convergence of the series degenerate into power one with exponent $5/3$. The surface $z = U(x, y)$ shown in Fig. 3.4 has been obtained without accelerating the convergence of the series. The stiffness coefficient C can also be calculated by formula (3.8). This coefficient is proportional to the volume bounded by the surface $z = U(x, y)$.

Table 3.4: The estimates C^+ and C^-

$\gamma = c/a$	1/2	1	2	3	4	9
$C^+/(16a^4G)$	0.571320	1.064226	1.874217	2.573292	3.246777	6.581903
$C^-/(16a^4G)$	0.571319	1.064225	1.874216	2.573290	3.246775	6.581901
$C^A/(16a^4G)$	0.580	1.0504	1.8436	2.5421	3.2152	6.5487

The estimates C^+ and C^- have been found by solving auxiliary systems of order $p = 30$ and are collected in Table 3.4 for different values of $\gamma = c/a$. According to the estimates, the first five to six significant digits are exact. The bottom row of the table contains approximate values of C^A from the monograph [3]. Comparing to the upper and lower bounds shows that their precision is one to two significant digits.

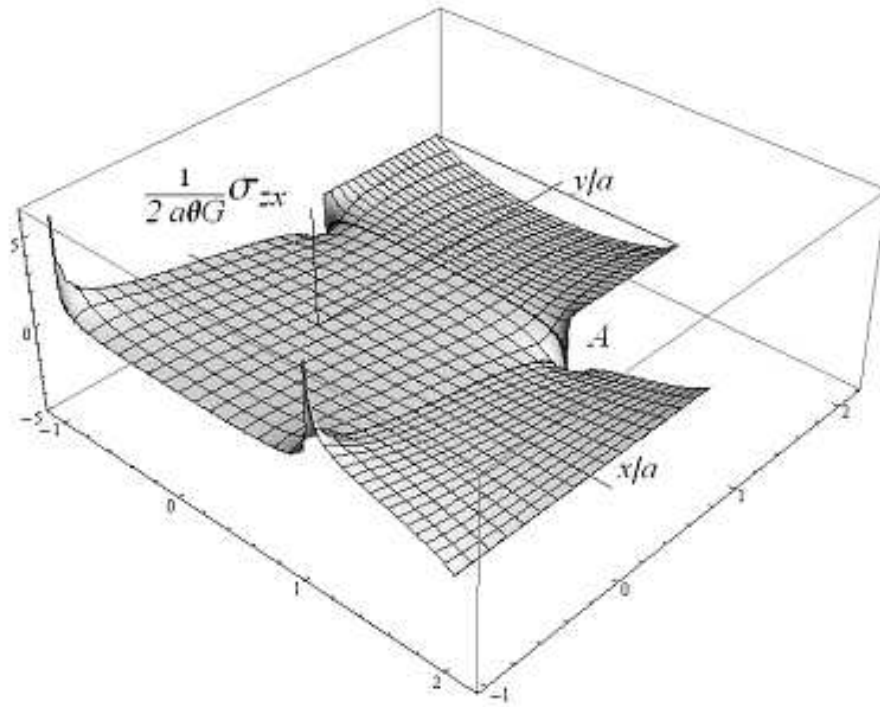


Figure 3.5: Surface $z = \sigma_{zx}(x, y)$

Difficulties arise when assessing the stresses that, according to (4.17), are proportional to the partial derivatives of the stress function with respect to the coordinates. On the boundary of the prism base where the stresses are maximum, the exponent of the Fourier coefficients is $2/3$. Figure 3.5 shows the surface $z = \sigma_{zx}(x, y)$ over the subdomains D_0, D_1 , and D_2 , which qualitatively demonstrates the distribution of tangential stresses. The surface $z = \sigma_{zx}(x, y)$ results from that in Fig. 3.5 turned in the plane of the prism base by a right angle. The neighborhood of the vertices of the reentrant angles (the point A in Fig. 3.5) and the neighborhoods of the intersection points between the prism base boundary and the coordinate axes x and y appear the most critical zones for the stress state. More critical are the neighborhoods of the intersection points because right angles in real structural elements are always rounded unlike

the idealized mathematical model used here. The rounding decreases the level of stress, which depends on the rounding curvature.

Improving the convergence of series (3.18) for the tangential stress $\sigma_{zx}(x, y)$ at the critical point ($x = f, y = 0$) leads to a formula whose principal part $8G/\pi^2$ coincides with that of a similar formula for a prism with a rectangular base D_1 (here G is Catalan's constant, $\gamma = c/a$);

$$\frac{1}{2aG\theta} \sigma_{zx}|_{x=f, y=0} = \frac{8}{\pi^2} \left(G + \sum_{n=1,3}^{\infty} \frac{(-1)^{\frac{n-1}{2}} \exp(-n\pi\frac{\gamma}{2})}{n^2 \sinh(n\pi\frac{\gamma}{2})} \right) + \sum_{n=1,3}^{2p-1} \frac{(-1)^{\frac{n-1}{2}} x_n}{n^{2/3} \sinh(n\pi\frac{\gamma}{2})}. \quad (3.43)$$

The sum of a Leibnitz-type series remaining in (3.43) can be estimated in an elementary way [10]. The bounds calculated by formula (3.43) are presented in Table 3.5 for different values of γ . The row of values of σ_{zy}^A from the monograph [3] are included for comparison. The difference between the upper- and lower-bound estimates for the maximum stresses is insignificant. For $\gamma \geq 9$, the stress is equal to the stress $8G/\pi$ in a rectangular-base prism.

The values in the bottom row of the table are in good agreement with the estimates in the neighborhood of $\gamma = 9$. In the neighborhood of $\gamma = 1$, however, the precision of the values in the bottom row reduces to one significant digit.

Figure 3.6 shows the stress σ_{zx} in the subdomain D_2 . These curves fall into two groups depending on their behavior. One group includes curves 5, 6, and 7 ($y = a + c/2, y = a + 3c/4$, and $y = f$, respectively) and characterizes the neighborhood of the point ($x = 0, y = f$) with the maximum stress σ_{zx} . The other group includes curves 1, 2, 3, and 4 ($y = a, y = a + c/100, y = a + c/30$, and $y = a + c/10$, respectively) and characterizes the neighborhood of the point A (the vertex of the reentrant right angle (Fig. 3.5)). The stresses increase abruptly in a small neighborhood of the point A. To plot curve 1 along which stresses tend to infinity as $x \rightarrow a$, the convergence of the series was improved by formulas (3.22) and (3.23). As a

Table 3.5: The estimates σ_{zy}^+ and σ_{zy}^- have been found by solving auxiliary systems

$\gamma = c/a$	1/2	1	2	3	4	9
$5\sigma_{zy}^+/(aG\theta)$	9.048541	8.839721	7.807063	7.507353	7.441889	7.424544
$5\sigma_{zy}^-/(aG\theta)$	9.048539	8.839719	7.807063	7.507353	7.441889	7.424544
$5\sigma_{zy}^A/(aG\theta)$	9.3331	8.929	7.8505	7.510	7.443	7.425

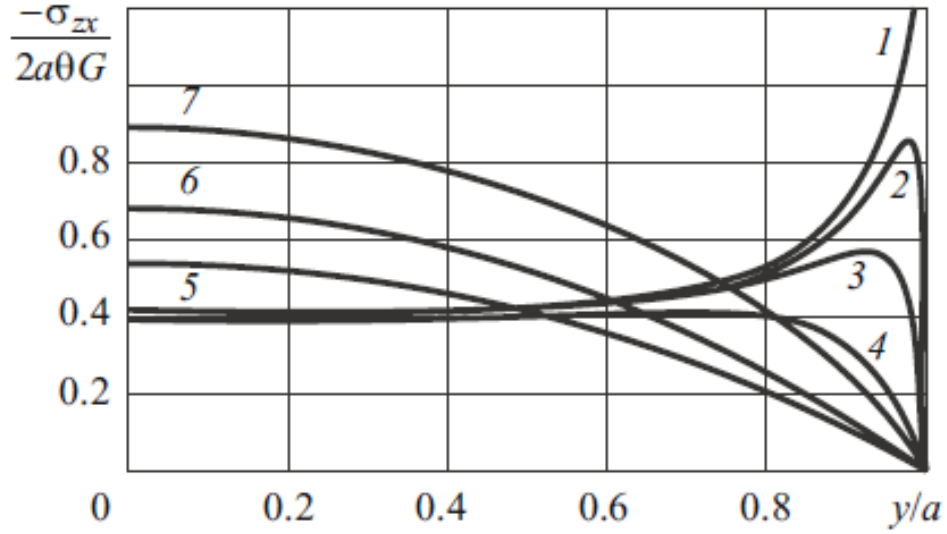


Figure 3.6: Stress σ_{zx} in the subdomain D_2

result, we obtain the formula

$$\begin{aligned} \frac{1}{2aG\theta} \sigma_{zx}^*|_{y=a} = & \sum_{n=1,3}^{2p-1} \left[\frac{H^{*p} - \coth(n\pi\gamma/2)}{n^{2/3}} - \frac{8}{n^2\pi^2 \sinh(n\pi\gamma/2)} \right] \sin\left(n\pi \frac{x+a}{2a}\right) \\ & + \frac{1}{2} H^{*p} \text{Im} \left[\text{Li}_{2/3}\left(-e^{i\pi \frac{x+a}{2a}}\right) - \text{Li}_{2/3}\left(e^{i\pi \frac{x+a}{2a}}\right) \right] \quad (0 \leq x \leq a), \end{aligned} \quad (3.44)$$

which together with the formula derived from (3.44) by replacing x_n and H^{*p} with x_n and h^{*p} allows us to estimate the lower and upper bounds for stresses on $y = a$.

In Figure 3.7 estimates the local perturbation of the stress state near the point A are given. These estimates have been obtained after improving the convergence of the series for $\sigma_{zx}(x, y)$ on $x = a$ ($0 \leq y \leq a$) based on (3.25). The following formula similar to (3.44) has been obtained:

$$\begin{aligned} \frac{1}{2aG\theta} \sigma_{zx}^*|_{x=a} = & \sum_{n=1,3}^{2p-1} \frac{y_n - H^{*p}}{n^{2/3}} \cos\left(n\pi \frac{y+a}{2a}\right) - \frac{y}{a} \\ & + \frac{1}{2} H^{*p} \text{Re} \left[\text{Li}_{2/3}\left(\exp\left(i\pi \frac{x+a}{2a}\right)\right) - \text{Li}_{2/3}\left(-\exp\left(i\pi \frac{x+a}{2a}\right)\right) \right]. \end{aligned}$$

Curves 1, 5 in Fig. 3.7 correspond to the following values of $\gamma = c/a$: $\gamma = 1/4, 1/2, 1, 2, 4$. It should be noted that all the curves in Fig. 3.7 are antisymmetric about the origin of coordinates.

Figure 3.7 leads us to the conclusion that the stress state is highly localized in a cross with short legs and high level of tangential stresses in a cross with long legs because the stress state

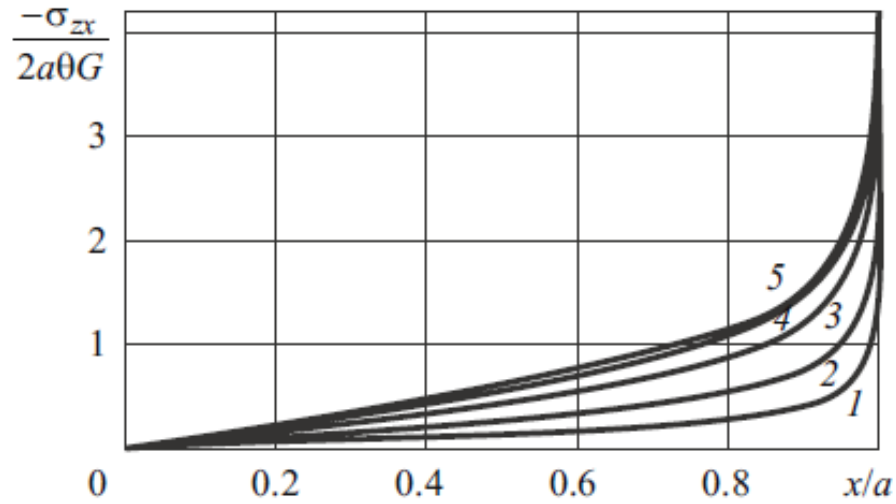


Figure 3.7: Local perturbation of the stress state near the point A

is less localized here. Note that the abruptly decreased difference between curve 4 ($\gamma = 2$) and curve 5 ($\gamma = 4$) is indicative of a limit point near curve 5.

Indeed, the curves with $\gamma > 4$ are hardly different from curve 5. The stress pattern near the point A remains almost the same for $\gamma \geq 4$.

CHAPTER 4

NUMERICAL METHOD

4.1 ALGORITHM OF SUCCESSIVE APPROXIMATION

Now we will consider the algorithm of successive approximation. This algorithm helps to obtain more accurate location of points M_j (M_{j^*}) on the boundary L . So this algorithm will let us build the approximate polynomial with the minimum deviation of L' from L .

Here is the sequence of steps:

1. Prestore some number of nodes $m = m_1$ and define somehow coordinates

$$z_{ja1}^{(0)} = x_{ja1}^{(0)} + iy_{ja1}^{(0)} \quad (4.1)$$

of nodes M_j of boundary L in a zero-approximation. These nodes we will mark as $M_{ja1}^{(0)}$ (see Fig. 4.1).

2. Take down points $M_{ja1}^{(0)}$ normally onto the curve L to prevent probable deflection. Let $M_{j1}^{(0)}$ ($z_{j1}^{(0)}$) be new points.

3. Compute coefficients using (2.13)

$$C_{k1}^{(0)} = \frac{1}{m_1} \sum_{j=1}^{m_1} z_{j1}^{(0)} e^{-ik\theta_j} \quad (k = 1, \dots, m_1) \quad (4.2)$$

of function (2.12)

$$z = \omega_{m_1}^{(0)}(\zeta) = \sum_{k=1}^{m_1} C_{k1}^{(0)} \zeta^k \quad (4.3)$$

in a zero-approximation. Here $\theta_j = \frac{2\pi}{m_1} j$ ($j = 1, \dots, m_1$).

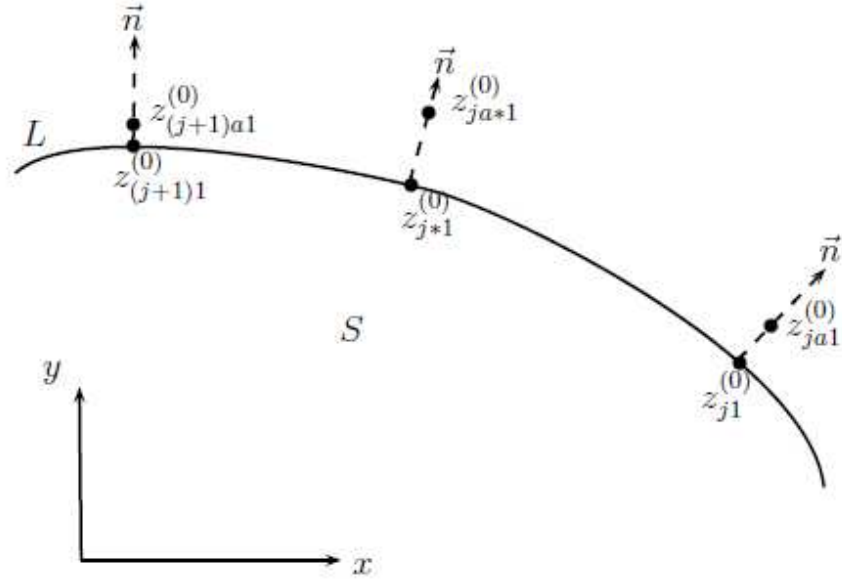


Figure 4.1: Take down points $z_{ja1}^{(0)}$ normally onto the curve L

4. Compute coordinates of $M_{ja^*1}^{(0)}$

$$z_{ja^*1}^{(0)} = \omega_{m_1}^{(0)}(e^{i\theta_j^*}). \quad (4.4)$$

These points correspond to intermediate nodes in a zero-approximation. Here $\theta_j^* = \frac{\pi}{m_1}(2j - 1)$ ($j = 1, \dots, m_1$). Note that these points are not necessary be on border L .

5. Take down points $M_{ja^*1}^{(0)}$ normally onto the boundary L . After that we will have points $M_{j^*1}^{(0)}$ with coordinates $z_{j^*1}^{(0)}$ ($j = 1, \dots, m_1$).

6. Using (2.19) lets compute coefficients

$$C_{k^*1}^{(0)} = \frac{1}{m_1} \sum_{j=1}^{m_1} z_{j^*1}^{(0)} e^{-ik\theta_j^*} \quad (k = 1, \dots, m_1). \quad (4.5)$$

of function (2.15)

$$z = \omega_{m_1}^{(0)}(\zeta) = \sum_{k=1}^{m_1} C_{k^*1}^{(0)} \zeta^k, \quad (4.6)$$

in a zero-approximation. Here $\theta_j^* = \frac{\pi}{m_1}(2j - 1)$ ($j = 1, \dots, m_1$).

7. Compute coordinates of $M_{ja1}^{(1)}$

$$z_{ja1}^{(1)} = \omega_{m_1}^{(0)}(e^{i\theta_j}) \quad (j = 1, \dots, m_1).$$

These points correspond to main nodes in a first approximation. Note that these points do not necessary be on border L .

8. Take down points $M_{ja1}^{(1)}$ normally onto the boundary L . After that we will have points $M_{j1}^{(1)}$ with coordinates

$$z_{j1}^{(1)} = x_{j1}^{(1)} + iy_{j1}^{(1)} \quad (j = 1, \dots, m_1).$$

Let these points are a first approximation of points M_j . Then starting from step number 3 we will repeat the algorithm until nodes $M_{j*1}^{(\lambda)}$ coincide with $M_{j*1}^{(\lambda-1)}$.

9. Finally we get polynomial

$$z = \omega_{m_1}^{(\lambda)}(\zeta) = \sum_{k=1}^{m_1} C_{k1}^{(\lambda)} \zeta^k.$$

This polynomial can be controlled by building big amount N of points of border L' . The equation for L' will be $\omega_{m_1}^{(\lambda)}(e^{i\theta})$.

10. Let Δ be a deflection of L' from L , where L is boundary of S . If Δ less then permissible value ε and curve L' does not have double points and cusps then finish the algorithm.

11. If deflection Δ is grater then permissible value then amount of nodes is doubled $m_2 = 2m_1$ and the algorithm starts from step 1. New zero-approximation for main nodes will be M_{ja2}^0 ($j = 1, \dots, m_2$)

$$z_{ja2}^{(0)} = \omega_{m_1}^{(\lambda)}(\zeta) = \sum_{k=1}^{m_1} C_{k1}^{(\lambda)} e^{ik\theta_j} \quad (j = 1, \dots, m_2)$$

where

$$\theta_j = \frac{2\pi}{m_2} j \quad (j = 1, \dots, m_2).$$

We will double the amount of nodes until the polynomial

$$z = \omega_{m_l}^{(\lambda)}(\zeta) = \sum_{k=1}^{m_l} C_{kl}^{(\lambda)} \zeta^k$$

satisfies the condition: the deflection Δ of a curve with parametric equation $z = \omega_{m_l}^{(\lambda)}(e^{i\theta})$ from the border L of domain S is less then permissible value.

After that we can reduce number of interpolation nodes (power of interpolation polynomial). Reduced number of nodes should be in the range $(\frac{m_l}{2}, m_l]$ but only if it is met the condition $\Delta < \varepsilon$.

Calculations are made in such way:

(a) Let new m_{l+1} be $m_l - 1$

(b) Calculate coordinates of nodes $M_{ja(l+1)}^{(0)}$

$$z_{ja(l+1)}^{(0)} = \omega_{m_l}^{(\lambda)}(e^{i\theta_j}),$$

where

$$\theta_j = \frac{2\pi}{m_{l+1}} j \quad (j = 1, \dots, m_{l+1}).$$

(c) Take down points $M_{ja(l+1)}^{(0)}$ normally onto the boundary L . Also make the sequence of approximations 2 - 7.

(d) Control resulting polynomial by condition

$$\Delta < \varepsilon.$$

If $\Delta < \varepsilon$ then let

$$m_{l+2} = m_{l+1} - 1$$

and so on starting from step (b) till we find minimal number of nodes m . This number m should satisfy the condition $\Delta < \varepsilon$.

Let sequence of steps 2 – 7 be inner circle. In inner circle the number of interpolation nodes does not change. Let sequence of steps in which the number of interpolation nodes is changed (decreased or increased) be outer circle. Now it is understood the notation: upper index of z or C_k corresponds to number of inner circles; the last digit of lower index corresponds to number of outer circles.

4.2 IMPROVEMENTS

Please note that conformal map which is built by previously described algorithm can be used for solving of boundary value problems(e.g. in theory of elasticity).

As for theory of elasticity local deflections of boundary L' from boundary L will seriously effect on local stress on boundary. These local disturbances of stress field are caused uppermost not by deflection Δ of boundary L' from given L but they are caused by distortion of radius of

curvature. And this is true because boundary L' has form of wave curve which passes main or intermediate interpolation nodes. In case of wave curve the radius of curvature of boundary L' changes in wide range. For complex curve L the radius of curvature can change it's direction twice in the range of single step.

According to [11] the function

$$z = \omega(\zeta) = \sum_{k=1}^m \tilde{C}_k \zeta^k, \quad (4.7)$$

where

$$\tilde{C}_k = \frac{C_k + C_{k^*}}{2} \quad (k = 1, \dots, m)$$

has same disadvantage. The curve L'' corresponding to function (4.7) has nearly twice smaller deflection Δ but boundary L'' saves it's form.

Because of local distortions of boundary for coefficients C_k or C_{k^*} as well as for coefficients \tilde{C}_k there are essential errors in determining of stress in boundary points. These errors can reach 50 ÷ 80% (and even more) as compared with the exact solution for curve L . It also is easy to see that increasing of power of mapping function will not correct this situation.

We can increase the accuracy of boundary L' and accuracy of solution for boundary-value problem by a simple transformation – the integral averaging. We will apply this transformation to approximate solution on interval $\theta - \frac{\pi}{m} \leq \theta \leq \theta + \frac{\pi}{m}$ which is equal to one step of interpolation. So we have:

$$z = \tilde{\omega}_n(\zeta) = \frac{m}{2\pi} \int_{-\frac{\pi}{m}}^{\frac{\pi}{m}} \omega_n[\rho e^{i(\theta+t)}] dt \quad (4.8)$$

It is good to use here function $\tilde{\omega}_n(\zeta)$ according to (4.7) because the corresponding curve L'' has deflections to both sides of the curve L . After integration we get

$$\begin{aligned} z = \tilde{\omega}_n(\zeta) &= \frac{m}{2\pi} \int_{-\frac{\pi}{m}}^{\frac{\pi}{m}} \sum_{k=1}^m \tilde{C}_k \rho^k e^{ik(\theta+t)} dt = \frac{m}{2\pi} \sum_{k=1}^m \left[\tilde{C}_k \zeta^k \int_{-\frac{\pi}{m}}^{\frac{\pi}{m}} e^{ikt} dt \right] = \\ &= \sum_{k=1}^m C_k \zeta^k \frac{\sin k \frac{\pi}{m}}{k \frac{\pi}{m}} = \sum_{k=1}^m D_k \zeta^k. \end{aligned} \quad (4.9)$$

Here

$$D_k = \tilde{C}_k \sigma_k \quad (k = 1, \dots, m), \quad (4.10)$$

where σ_k ($k = 1, \dots, m$) – weighting coefficients, which are defined by

$$\sigma_k = \frac{\sin k \frac{\pi}{m}}{\frac{\pi}{m}} \quad (k = 1, \dots, m). \quad (4.11)$$

The border of L''' , which corresponds to (4.9), is nearly to match border L . This means that L''' has deflection from L much less than curves L' and L'' . But the biggest advantage is that errors in radius of curvature are not more than $5 \div 10\%$. In the same time curves L' and L'' could not be compared with curve L in the sense of radius of curvature. On the one step of interpolation these curves (L' and L'') could change not only magnitude but also a sign of curvature.

Please note that the operation of integration is applied to all approximate expressions of conforming map. And because of this, in future, we will not distinguish between denotes for coefficients of $\tilde{\omega}_n(\zeta)$ and $\omega_n(\zeta)$. Even after the essential increasing of accuracy of the border of S' (using weighting coefficients (4.11)) local distortions of the field of stresses partly can be saved.

On the other hand the real machine elements and structural members are made with some tolerance of the form. This means that real boundary does not match the ideal boundary L .

4.3 SYMMETRICAL PROFILE CASE

It is usual case when we need to solve a particular problem for a profile which has one or more (q) symmetry axes. Let's choose the coordinate origin in the point where symmetry axes cross. Coordinate axis' x direction will match one of these symmetry axes. Then interpolation polynomial which agrees with mapping function on interval $0 \leq \theta \leq \frac{\pi}{q}$ in interpolation nodes $\zeta = \zeta_j = e^{i\theta_j}$, where $\theta_j = \frac{\pi}{qm_1}j$ ($j = 0, \dots, m_1$) will be

$$z = \omega_{m_1}(\zeta) = \sum_{k_1=0}^{2m_1-1} d_{qk_1+1} \zeta^{qk_1+1}. \quad (4.12)$$

Here coefficients $d_k = d_{qk_1+1}$ are real. The formulas for d_k can be easily found from (2.13):

$$d_k = \frac{1}{m_1} \left\{ \frac{1}{2} [|z_0| + (-1)^{\frac{k-1}{q}} |z_{m_1}|] + \sum_{j=1}^{m_1-1} \left(x_j \cos \frac{\pi}{qm_1}kj + y_j \sin \frac{\pi}{qm_1}kj \right) \right\}, \quad (4.13)$$

$$k = 1, q+1, \dots, (2m_1-1)q+1,$$

where $z_j = x_j + iy_j$ are coordinates of nodes M_j of the border L . Here L is a border of domain S . Nodes ζ_j ($j = 0, \dots, m_1$) from a unit disk after the conformal map are transformed to M_j the interpolation nodes.

In the same way as for arbitrary profile form we can develop an algorithm of successive approximation. Let us build an interpolation polynomial:

$$z = \omega_n^*(\zeta) = \sum_{k_1=0}^{2m_1-1} d_{(qk_1+1)^*} \zeta^{qk_1+1}. \quad (4.14)$$

This polynomial will be equal to function $z = \omega(\zeta)$ in interpolation nodes $\zeta_j^* = e^{i\theta_j^*}$, where $\theta_j^* = \frac{\pi}{2qm_1}(2j-1)$ ($j = 1, \dots, m_1$). Coefficients $d_{k^*} = d_{(qk_1+1)^*}$ can be found from next formulas:

$$d_{k^*} = \frac{1}{m_1} \sum_{j=1}^{m_1} \left[x_{j^*} \cos \frac{\pi(2j-1)}{2qm_1} k + y_{j^*} \sin \frac{\pi(2j-1)}{2qm_1} k \right], \quad (4.15)$$

$$k = 1, q+1, \dots, (2m_1-1)q+1,$$

where $z_{j^*} = x_{j^*} + iy_{j^*}$ is the value of mapping function in interpolation nodes ζ_j^* .

The methodology for building of successive approximations for the symmetric profile is the same as for the general case but in case of symmetric profile we use other formulas (4.12) – (4.15).

4.4 SELECTION OF INITIAL APPROXIMATION

Let's consider a problem of selection of initial approximation.

We will consider two ways of solving this problem. Since we use described above algorithm for calculation these two ways are practically identical.

1. Usage of electrical simulation of conformal mapping for experimental determination of nodes of conformity of boundary L and boundary $|\zeta| = 1$ [42].
2. The numerical solution of the problem, starting from $m_1 = 2$, when one node $M_2^{(0)}$ is known exactly (it is defined by normalization). The second one $M_1^{(0)}$ can be selected arbitrary.

The second way of selection of initial approximation is trivial. Let us consider first way more detailed.

Conformal mapping of unit disc $|\zeta| < 1$ into domain S (under described above normalization conditions) behaves like this:

1) orthogonal net which consists of radii ($\theta = const$) and circles ($\rho = const$) of disc $|\zeta| < 1$ will be mapped into orthogonal net of lines which start at $z = 0$ and ending on the border L and closed lines $\rho = const$;

2) circle of infinitesimal radius $|\zeta| = \delta$ on plane ζ maps into circle of infinitesimal radius $|z| = \delta_1 = \delta|\omega'(0)|$ on plane z ;

The same situation can be simulated on electrical machine. This is because of properties of equivalent potential lines. It is known that equivalent potential lines and current lines make form orthogonal net in some conditions. Because of uniqueness of conformal map that orthogonal net will match the orthogonal net $\theta = const$ and $\rho = const$.

4.5 SOLUTION OF TORSION PROBLEM

As an example we will solve a torsion problem for the rod (prism) with the cruciform profile.

First let us consider the problem definition. Let us consider the rod (the prism solid) which has cruciform base. Length l between prism bases is much more greater than the base sizes. Also we add right-hand coordinate system $xOyz_1$. Superpose plane xOy with one of the prism bases and axes z_1 turn to center axis of a rod. Let us fix the base of rod (the same as lays in plane xOy). We will rule out travel of the fixed base as a unit but deformations are allowed. The center of forces on another base will be the node of intersection of z_1 and another base.

It is known that in case of torsion Hook's law expresses dependence of rotation angle ϕ on torsional moment M_T . Torsional moment M_T characterizes tangent directions σ_{zx}, σ_{zy} on base of prism

$$\phi = \frac{M_T l}{G J_T},$$

where l – prism height, G – modulus of rigidity, J_T – torsion constant.

The Hook's law can be written in such a way

$$\theta = \frac{M_T}{C}. \quad (4.16)$$

Here $\theta = \frac{\phi}{l}$ is the specific torsion angle, $C = GJ_T$ is the stiffness coefficient for torsion. The tangent directions in prism can be written using Prandtl's function of stresses $U(x, y)$

$$\sigma_{zx} = G\theta \frac{\partial}{\partial y} U; \sigma_{zy} = -G\theta \frac{\partial}{\partial x} U. \quad (4.17)$$

The Prandtl's function is defined by solution of Dirichlet's problem for Poisson's equation in domain D – the base of the prism

$$\frac{\partial^2}{\partial x^2} U + \frac{\partial^2}{\partial y^2} U = -2; \quad U|_{\Gamma} = 0. \quad (4.18)$$

Formulas (4.17) allow us to express torsional moment through stress function

$$M_T = 2G\theta \iint_D U dx dy. \quad (4.19)$$

After substitution of (4.19) into Hook's law 4.16 we get the formula for stiffness:

$$C = 2G \iint_D U dx dy. \quad (4.20)$$

We can see that the problem of torsion of the rod is equivalent to the solving of Poisson's equation. This differential equation is solved by method of conformal maps. Usage of this method simplifies solving of the problem of torsion. Solution of the problem can be evaluated using the conformal map which maps from unit disk ($|\zeta| < 1$) into given domain (in our case it is cruciform domain, Fig. 4.2). In general finding of such conform map is not trivial problem.

The most effective solution of boundary-value problem for simply connected domain can be produced when it is known the conformal map $z = \omega(\zeta)$ that maps from unit disk ($|\zeta| < 1$) into given domain S (in our case it is cruciform domain). We will search this conformal map as a polynomial (2.1) as it was described in Section 2.2.

Please note that in corners of profile conformity is violated, as it was mentioned in Section 2.1. This means that a polynomial (2.1) of a finite power will not provide us a conformal map in corners of a profile. Because of this the piecewise-smooth boundary should be transformed into curve with continuously changing tangent. In most of cases corners of the boundary can be rounded by arcs of the constant radius as it happens in real machine elements. In case of cruciform domain corners can be transformed into quarters of circles.

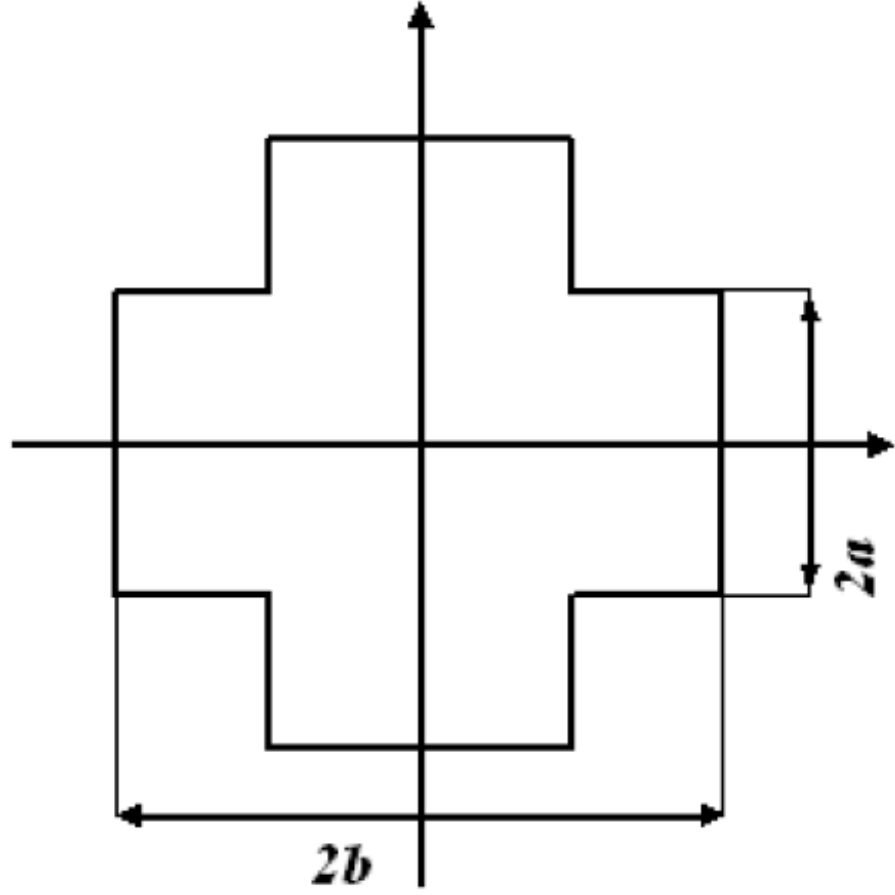


Figure 4.2: Cruciform profile

Using the coefficients of polynomial (2.1) which implements conformal mapping we can express tangential stresses on the border. Let

$$D_k = \sum_{r=1}^{m-k} C_{k+r} \bar{C}_r \quad (k = 0, \dots, m-1)$$

and

$$\begin{cases} B_{-k} = \sum_{r=1}^{m-k} r C_r \bar{C}_{r-k} \quad (k = 0, \dots, m-1), \\ B_k = k D_k + \bar{B}_{-k} \quad (k = 0, \dots, m-1). \end{cases}$$

Then tangential stress can be expressed as

$$\tau_\theta = \frac{\mu\tau}{|\omega'(\sigma)|} \left[B_0 + 2\operatorname{Re} \left(\sum_{k=1}^{m-1} \bar{B}_{-k} \sigma^k \right) \right].$$

Torsional stiffness

$$D = \mu \frac{\pi}{2} \left\{ B_0 D_0 - \sum_{k=1}^{m-1} k |D_k|^2 + 2\operatorname{Re} \left(\sum_{k=1}^{m-1} D_k B_{-k} \right) \right\}.$$

There is one feature described in [43] – the selection of way for deflection nodes. In case of cruciform profile (in which corners are rounded by quarters of the circle) deflection is made through the perpendicular to tangent.

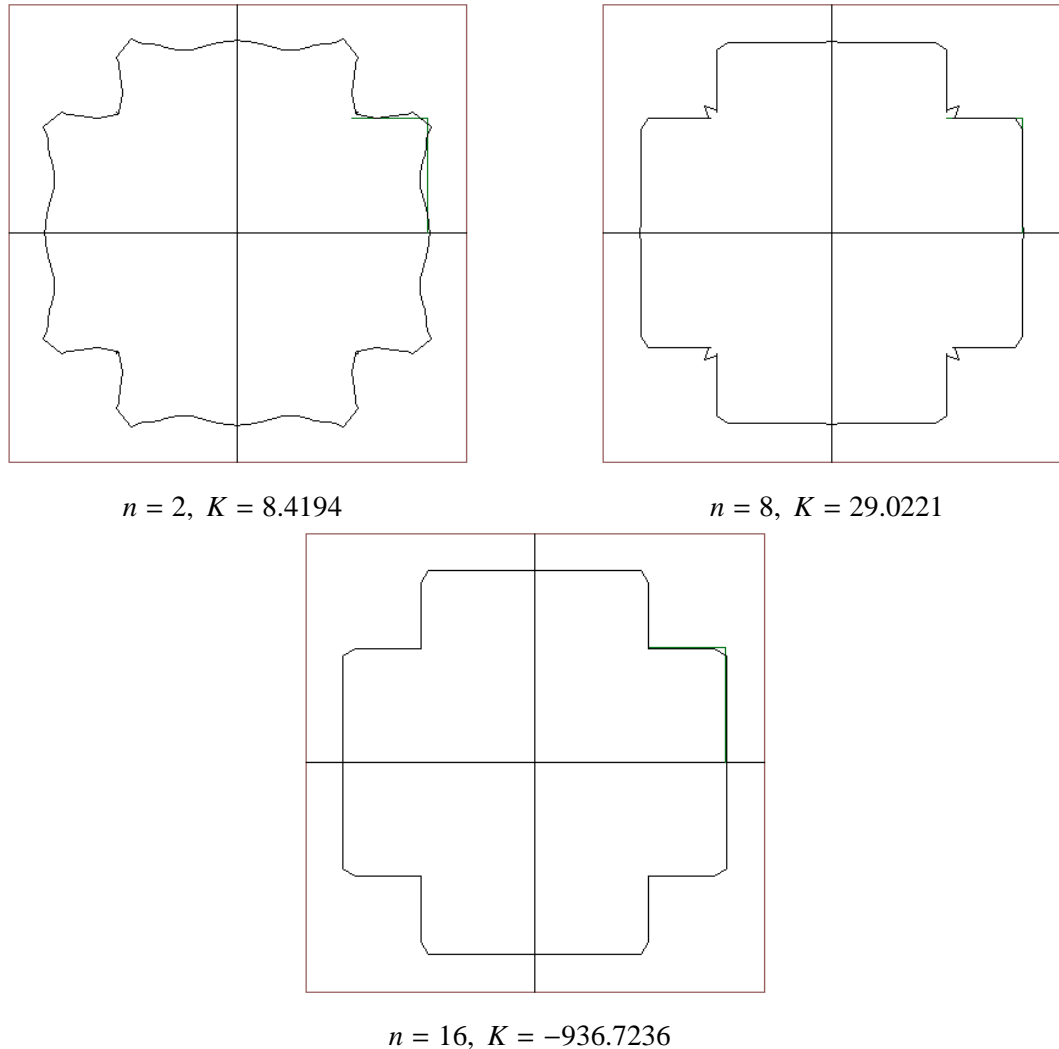


Figure 4.3: Algorithm of successive approximations

On Figure 4.3 it is shown the working process of algorithm of successive approximation for solving of torsion problem for the rod with the cruciform profile. Here n is a number of steps in algorithm. The curve shown on the figures is a graph of polynomial that implements conformal map. It can be seen that with increasing of number of steps curve comes closer to border of profile.

Also it is interesting to check not only matching of curve forms but also radius of curvature

in inner corner K . The curvature in inner corner is calculated from such a formula

$$K|_L = \frac{1}{|\omega'(\sigma)|} \left[1 + \operatorname{Re} \left(\frac{\sigma \omega''(\sigma)}{\omega'(\sigma)} \right) \right]$$

and radius of curvature is inverse value

$$r = \frac{1}{K}.$$

In case of our example we rounded corners of the profile with the quarters of circles with the radius $r = \frac{1}{K} = 10^{-3}$. So we can also see that the radius of curvature also converges to the real radius of profile when number of steps increases.

Also we investigated dependence of stress in inner corners on radius of rounding arcs. This dependence is shown on the Plot 4.4. In this figure the abscissa is the rounding radius and ordinate is stress value. This plot was developed for profile with the size $d = 2a$ (please see Fig. 4.2).

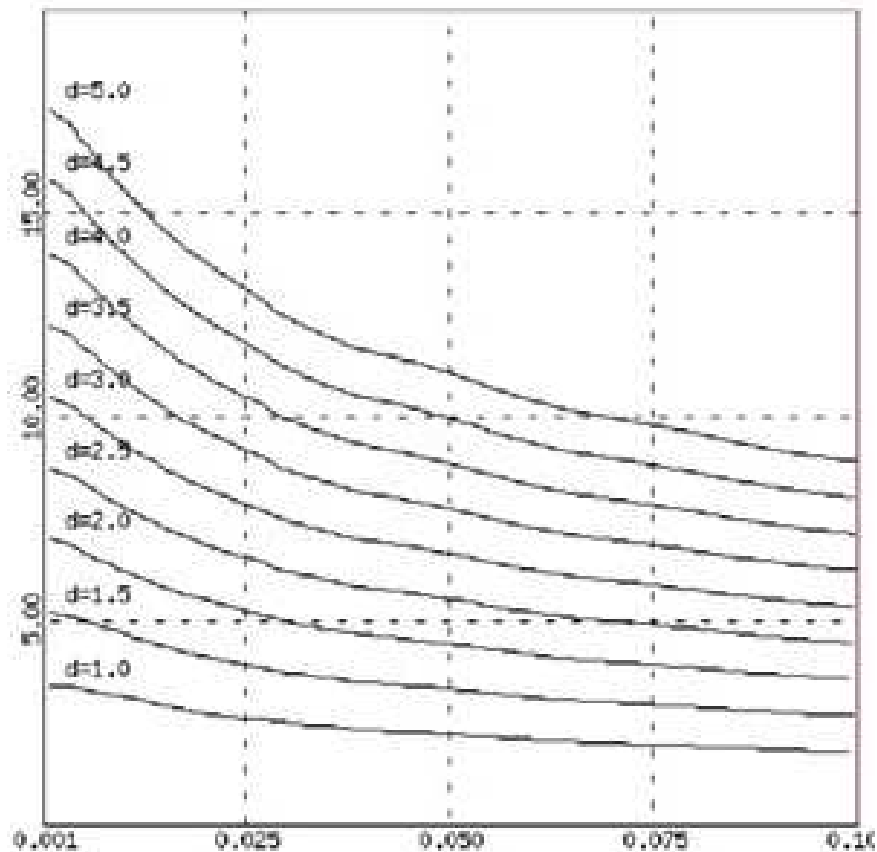


Figure 4.4: Dependence of stress in inner corner on radius of curvature

CHAPTER 5

COMPARISON AND CONCLUSIONS

In this thesis we introduced a numerical method for conformal mapping based on algorithm of successive approximations. In Table 5.1 a comparison of values of stiffness coefficient calculated by the Chekhov's method described in the chapter 3 (upper C^+ and lower C^- estimates) and values C^K found by conformal maps method (given values are calculated for the cross-shaped domain with rounded corners). The bottom row of the table contains approximate values of C^A from the monograph [3]. In Fig. 5.1 you can see the relative error estimation graph for conformal map method (solid line) and Abramyan's method (dashed one).

Please note that estimation of stiffness coefficient in [3] is very crude. Maybe this error of estimator ensue from errors in calculation, e.g. accumulated rounding error on old computers. As for Chekhov's method we consider it results to compare with results obtained with the help of conformal map method. Chekhov's estimation is considered as the exact (analytical) solution of the torsion problem for the cross-based (with the right angles) prism.

We should note that estimate C^K obtained by conformal map method is less then lower Chekhov's estimate C^- which are calculated for the cross-shaped (without rounded corners) domain. This can be explained by the fact that according to (4.20) the value of stiffness

Table 5.1: Comparison of exact and numerical solutions

$\gamma = c/a$	1/2	1	2	3	4	9
$C^+/(16a^4G)$	0.571320	1.064226	1.874217	2.573292	3.246777	6.581903
$C^-/(16a^4G)$	0.571319	1.064225	1.874216	2.573290	3.246775	6.581901
$C^K/(16a^4G)$	0.570416	1.063575	1.863686	2.571791	3.238395	6.571751
$C^A/(16a^4G)$	0.580	1.0504	1.8436	2.5421	3.2152	6.5487

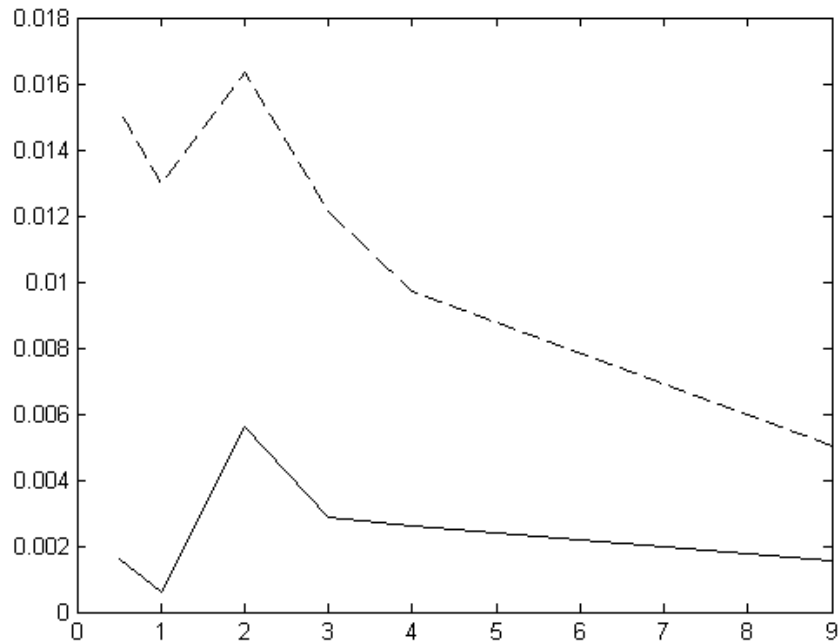


Figure 5.1: Relative error estimation

coefficient is directly proportional to the volume bounded by the surface $z = U(x, y)$.

Also please note that the introduced conformal map method (see Section 2.2) is really convenient. As we said above this method can be easily applied in practical usage, e.g. in engineering calculations. This is because of property of real world machine elements have no right angles. Instead of right angles there is some curve which can be easily approximated by arcs of finite radius.

Another practical advantage of the conformal map method is relatively easy way of program implementation. Convenience in programming is because of modules (libraries with the set of functions) written for the prism with the specific base are easily extended and adapted to new complex domains. Especially the core algorithm functions are not changed for all simply connected domains but it is only changed the algorithm of fetching down of nodes.

And the main advantage of the conformal map method consists of the fact that for most of complex simply connected domains analytical solution cannot be found. Or even if it is found that it is hard to use it in practice. But numerical solution found by conformal map method can be easily found and used (e.g., in engineering calculations)

REFERENCES

- [1] Abramyan B.L., Torsion of prismatic rods with a cross-shaped cross section, *Prikl. Mat. Mekh.*, 13, No. 5, 1949, 551-556
- [2] Arutyunyan N.Kh., Solving the problem of torsion of rods with polygonal cross section, *Prikl. Mat. Mekh.*, 13, No. 1, 1949, 107-113
- [3] Arutyunyan N.Kh., Abramyan B.L., Torsion of elastic bodies Moskow, *Fizmatgiz*, 1963 (Russian)
- [4] Baltrukonis, Chi M., Laura P.A.A., Axial shear vibrations of star shaped bars – Kohn-Kato bounds. Eighth Midwestern Mech. Conf., *Developments in Mech.* 4, 1965, 449-467
- [5] Bermant A.F., Markushevich A.I. The theory of complex variable functions Digest *The mathematics in USSR for 30 years*. M.-L., Gostehizdat, 1948, 319-480. (Russian)
- [6] Casarella M.J., Laura P.A.A., Chi M., Ferragut N., On the approximate solution of flow and heat transfer through non-circular conditions with uniform wall temperature and heat generation. *Nucl. Engg. Design* 16, 1971, 387-398
- [7] Chekhov V.N, Pan A.V., Limiting expressions for Koyalovich's limitants, *Dop. NAN Ukrainy*, No. 3, 2007, 31-36
- [8] Chekhov V.N., Stress state of a cross-base prism under torsion *Int. Appl. Mech.* 44, No. 11, 2008, 1265-1278
- [9] Deresieicz H., Thermal stress in a plate due to disturbance of uniform heat flow in a hole of general shape. *J. Appl. Mech.*, Trans. *ASME* 28, 1961, 147-149
- [10] Fikhtengol'ts G.M., A Course of Differential and Integral Calculus, Vol. 2 Moscow, *Fizmatgiz*, 1962 (Russian).
- [11] Filchakov P.F. Approximate methods for conformal mapping. Kyiv, *USSR*, 1964 (Russian).
- [12] Florence A.L., Goodier J.N., Thermal stress due to disturbance of uniform heat flow by an insulated ovaloid hole. *J. Appl. Mech.*, Trans. *ASME* 27, 1960, 635-639
- [13] Govurin M.K., Kantarovich L.V. Approximate and numerical methods. Digest *The mathematics in USSR for 40 years*. M., *Fizmatgiz*, 1959, 846-848 (Russian).
- [14] Grinchenko V.T., Equilibrium and Steady-state vibrations of finite-size elastic bodies, Kyiv, *Naukova Dumka*, 1978 (Russian)
- [15] Grinchenko V.T., Meleshko V.V., Harmonic vibrations and waves in elastic bodies, Kyiv, *Naukova Dumka*, 1981 (Russian)

- [16] Guz A.N., Shnerenko K.I., Analyzing infinite systems of equations for finite multiply connected domains in shells, *Theory of plates and shells*, Nauka, Moskow, 1949, 311-315 (Russian)
- [17] Inoue K., Grid generation for cascades using conformal mapping. *J. Comput. Phys.* 52, 1983, 130-140
- [18] Inoue K., Grid generation for inlet configurations using conformal mapping. *J. Comput. Phys.* 58, 1985, 146-154
- [19] Ives D.C., A modern look at conformal mapping including multiply connected regions. *AIAA J.* 14, 1976, 1006-1011
- [20] Kayuk Ya.F., Stress state of flexible plates with a hole that are subject to bending *Int. Appl. Mech.* 43, No. 1, 2007, 85-100
- [21] Kantarovich L.V, Krilov V.I. Approximate methods of higher analysis. M.-L., *Fizmatgiz*, 1962 (Russian).
- [22] Koyalovich B.M., Analysis of infinite systems of linear algebraic equations *Izv. Fiz.-Mat. Inst. im. V. A. Steklova* No. 3, 1930, 41-167 (Russian).
- [23] Koppenfels V., Shtalman F. The practice of conformal mapping. M., *II*, 1963 (Russian).
- [24] Kythe P. Computational conformal mapping. *Birkhäuser*, Boston, 1998
- [25] Laura P. A. A., A survey of modern applications of the method of conformal mapping. *Revista de la Union Mathematica Argentina* 27, 1975, 167-179
- [26] Laura P.A.A., Chi M., Approximate method for the study of heat conduction in bars of arbitrary cross section. *J. Heat Transfer, Trans. ASME* 86, Ser. C, 1964, 466-467
- [27] Laura P.A.A., Shahady P.A., Longitudinal vibrations of a solid propellant rocket motor. Proc. Third Southeastern Conf. on Theor. Appl. Mech., *Pergamon press*, New York, 1966, 623-633
- [28] Meleshko V.V., Bending of an elastic rectangular clamped plate: exact versus 'engineering' solutions *J. Elasticity* 48, No. 1, 1997, 1-50
- [29] Meleshko V.V., Superposition method in thermal-stress problems for rectangular plates *Int. Appl. Mech.* 41, No. 9, 2005, 1043-1058
- [30] Menikoff R., Zemach C., Methods for numerical conformal mapping. *J. Comput. Phys.* 36, 1980, 366-410
- [31] Menikoff R., Zemach C., Rayleigh-Taylor instability and the use of conformal maps for ideal fluid flow. *J. Comput. Phys.* 51, 1983, 28-64
- [32] Muskhelishvili N.I., Some basic problems of the mathematical theory of elasticity. Moskow, *Singular integral equations*, 1946 (Russian)
- [33] Papkov S.O., Studying the singularities of the stress state of an angle under torsion *Uch. Zap. Simferopol'skogo Gos. Univ.* No. 5 (44), 1998, 75-79 (Russian)
- [34] Prudnikov A.P., Brychkov Y.A., and Marichev O.I., Integrals and Series. Elementary Functions *Nauka*, Moskow, 1981. (Russian)

- [35] Siegel R., Goldstein M.E., Savino J.M., Conformal mapping procedure for transient and steady state two-dimensional solidification. *Heat Transfer*, Elsevier, Amsterdam, 1970
- [36] Shaldyrvan V.A., Some results and problems in the three-dimensional theory of plates (review) *Int. Appl. Mech.* 43, No. 2, 2007, 160-181
- [37] Shnerenko K.I., Godzula V.F., Stress state of a cylindrical composite panel weakened by a circular hole *Int. Appl. Mech.* 42, No. 5, 2006, 555-559
- [38] Shulga N.A., Effective magnetoelastic properties of laminated composites *Int. Appl. Mech.* 42, No. 8, 2006, 879-885
- [39] Sparrow E.M., Haji-Sheikh A., Flow and heat transfer in ducts of arbitrary shape with arbitrary thermal boundary conditions, *J. Heat Transfer*, trans. *ASME* 88, 1966, 351-356
- [40] Trefethen L.N. (ed.), Numerical conformal mapping. *North-Holland*, Amsterdam, 1986
- [41] Ugodchikov A.G., The building of conformal map using the electro modelling method and Lagrange interpolation polynomials. Kyiv, *Naukova dumka*, 1966. (Russian)
- [42] Ugodchikov A.G. et al., Solution of boundary-value problem in plane elasticity theory using digital and analog machines. Lagrange interpolation polynomials. Moscow, *Visshaya shkola*, 1970. (Russian)
- [43] Ugodchikov A.G., Shvetsov A.V., Botov V.A., About new methodology for deflection of outline nodes in conformal mapping, *Applied mechanics*, 9, No. 11., 1973 (Russian)